University of Alberta

Coupling of Stress Dependent Relative Permeability and Reservoir Simulation

by

Samuel Ojagbohunmi

A thesis submitted to the Faculty of Graduate Studies and Research
in partial fulfillment of the requirements for the degree of

Master of Science
in
Petroleum Engineering

Department of Civil and Environmental Engineering

Spring 2012
Edmonton, Alberta

Abstract

Geomechanics is increasingly being considered for inclusion in reservoir simulation, since conventional simulators do not honor deformation resulting from the interaction between stress and fluid flow response in a porous medium. Most of the recently developed sequentially coupled approaches for coupling flow and geomechanics have focused on updating porosity and absolute permeability while changes in relative permeability (due to geomechanics) is ignored. For multiphase flow systems, relative permeability functions are one of the most influential parameters controlling fluid movement and distribution. To examine how geomechanically-influenced relative permeability may impact flow, a sequentially coupled reservoir geomechanical simulation study was conducted. The simulation workflow incorporated automatic updates of the relative permeability table for each grid block in the model at every time-step. Data for populating the geomechanical relative permeability tables was extracted from recent experimental test results reported in the literature.

Results from the simulation studies showed a significant difference in recovery factors when the impact of geomechanics on relative permeability functions was integrated into coupled simulation compared to when only changes in porosity and absolute permeability were used.

Coupled models which incorporate not only the change in permeability and porosity but also the changes in relative permeability can lead to more realistic production forecast especially for reservoirs under improved or enhanced oil recovery scheme as found in heavy oil and oil sands projects.

Acknowledgement

This thesis would not have been possible without the support and guidance of some individuals who in one way or another contributed and extended their valuable assistance towards the completion of this study. First and foremost, I want to thank God for the gift of life, the wonderful opportunities and the grace to complete this study.

I am heartily thankful to my supervisor Dr. Rick Chalaturnyk for his encouragement, guidance and support from the start to the end of the study. I really appreciate all his contributions of time, ideas and funding to make my M.Sc. experience productive and interesting. It was indeed a great honor to have been part of the Reservoir Geomechanics Research Group.

I would also like to thank my co-supervisor Dr. Juliana Leung for her valuable contributions to the completion of this study.

I am much indebted to Nathan Deisman for his help with the code used in coupling IMEX and FLAC 3D, and above all for his support. I also benefited by advice and guidance from Nathan who always grants me his time without hesitation.

Lastly, I am grateful to my family for their sacrifices and understanding during the period of this study.

Table of Content

List of Tables

List of Figures

Nomenclature

A, B	Constants in approximate shape of the relative permeability curve
Bo	Oil formation volume factor, m^3/m^3
Boi	initial oil formation volume factor, m^3/m^3
bi	Body force per unit mass
E	Young's modulus, Pa
G	Shear modulus, Pa
K	Bulk modulus, Pa
k	Fracture gradient constant
k_r	Effective permeability of each phase
k_{ri}	Relative permeability of each phase
k, k_o	Current and initial absolute permeability
k_{ro}	Relative permeability to oil
k_{roo}	Relative permeability to oil at original in-situ stress
k_{ro}^*	Normalised relative permeability to oil
$k_{ro}(S_{wir})$	End point relative permeability to oil at irreducible water saturation
k_{rw}	Relative permeability to water
k_{rwo}	Relative permeability to water at original in-situ stress
k_{rw}^*	Normalised relative permeability to water
$k_{rw}(S_{or})$	End point relative permeability to water at residual oil saturation

n_o, n_w	Corey oil and water exponent
P_{cog}, P_{cow}	Oil-gas and oil-water capillary pressure
P_g, P_o, P_w	Pressure in the gas, oil and water zone respectively
P_p	Pore pressure
R_s	Solution gas-oil ratio
S_g	Gas saturation
S^*, S_{wn}	Normalised water saturation
S_{on}	Normalised oil saturation
S_o, S_w	Oil and water saturation
S_{or}, S_{wc}	Residual oil and connate water saturation
S_{oro}	Residual oil saturation at original in-situ stress
S_{or}^*	Normalised Residual oil saturation
S_{wir}	Irreducible water saturation
S_{wiro}	Irreducible water saturation at original in-situ stress
S_{wir}^*	Normalised irreducible water saturation
S_{wcit}	Critical water saturation
q_o,q_w,q_g	Rate of oil, water and gas, m^3
ϕ, ϕ_o	Current and initial porosity
ϕ^*	Porosity multiplier
ε_v	Volumetric strain, Pa
$\varepsilon_{xx}, \varepsilon_{yy}, \varepsilon_{zz}$	Axial strains, Pa
γ	Density in terms of pressure/distance
μ_o, μ_w	Oil and water viscosity

u	Displacement
ν	Poisson's ratio, dimensionless
∂z	Vertical depth increment, m
g	Acceleration due to gravity, m/sec^2
$\overset{-}{\sigma}$	Co-rotational stress-rate tensor
κ	Parameter that takes into account the history of loading
$\rho_m, \rho_{fl}, \rho_b$	Matrix, fluid and bulk density, g/cm^3
ξ_{ij}	Strain rate tensor
υ_{ij}	Translation velocity
ρ	Density of the medium, g/cm^3
σ_v	Vertical stress, Pa
$\sigma_{ij}^{'}$	Effective stress, Pa
σ_{ij}	Total stress, Pa
α	Biot Coefficient, dimensionless
$\Delta\sigma_{i,j}$	Change in total stress, Pa

Chapter 1

Introduction

1.1 Background

More than ever, oil companies around the world are faced with problems of declining reserves, identification of next new business platform, harsh business environments in some countries where oil and gas assets are located and the search for a sustainable blueprint for future growth and success. Road-mapping exercises in view of these challenges had led to the development of business opportunities especially in the deep offshore, as well as well as increased unconventional petroleum resource exploitation, as companies are pushed to stretch beyond the self-limiting boundaries of current technology.

Considering the huge cost of production from these assets, the current concerns are focused more in planning and the process of decision making. Of central concern are: determination of the most worthy place to invest, surveying of all options, selecting the best one and allocate resources to the projects that have the most favorable potential, considering the economics and impacts on the environment.

Increasingly, companies are now depending more heavily on the use of numerical and lab scale experimental models to assess risk inherent in their business; reducing uncertainties and ultimately optimizing the economics benefit using pilot project before moving to commercial phase.

Models can be used to obtain long term development plans, however, the selection of the appropriate model or combination of models is fundamental for optimal depletion strategy for a given reservoir asset. This is critical for the optimization of management's decision to develop the asset at early stage and the improvement of the overall amount of recoverables. Consequently, it is crucial to have a model that accurately depicts the processes taking place in the reservoir. In other words, every parameter influencing both fluid and rock displacement and their impact on the recoverable reserves during primary, secondary and tertiary recovery stage should be accounted for in the model.

In addition, as production data becomes available, models need to be validated and updated. Validating or reducing uncertainty in reservoir models rely heavily on availability of data for accuracy in performance forecast. When production history is available, pressure and saturation distribution existing laterally and vertically in a field, as well the observed water cuts and gas oil ratios both on a field scale and on well level can be incorporated via history matching to characterize the reservoir uncertainty. This history matching ensures, future performance forecast are made using the model with a full confidence that the geologic, petrophysical, mechanical and fluid parameters accurately portray all the pertinent flow physics.

Thus, a reliable production forecast depends on; properly defining the reservoir volume allocated to hydrocarbon, transmissibility, total energy in the reservoir and how that energy is distributed; as well as characterizing the movement of water and free gas relative to oil. For multiphase flow systems,

relative permeability is one of the most influential parameter controlling fluid movement and distribution. It is an important property used by the standard reservoir simulator to represent the interaction between rock and fluid.

1.2 Statement of the Problem

Geomechanical behavior of porous media has become increasingly important to hydrocarbon operations, (Settari and Walters, 1999). As reservoirs experience voidage or changes from one recovery mechanism to another, there are associated changes in pore pressures and in-situ stresses. The volumetric response these changes induce in the reservoir rock depends on the geomechanical properties of the rock and the combined effect of changes in pore pressure and stress state (Jose, 1998). Depletion in reservoir pore pressure due to production can cause significant deformation, including compaction, porosity and permeability loss, especially in unconsolidated and weak formations (Zoback, 2007). Equally, the injection of water into a reservoir changes the pore pressure and the stress state, potentially causing dilation of the rock matrix. Dilation increases porosity, permeability, alters water saturation, fluid mobility, and pressure distribution.

The behavior of reservoir pore space during geomechanical process can be illustrated using scanning electron microscope (SEM) micrograph of the nanotunex shown in Figure 1.0. Isotropic compression on the nanotunex will cause shrinkage of the pore body and pore throat's surface area analogous to the process leading to reduction in reservoir pore space and connectivity. While

isotropic unloading by pore pressure injection could results to enlargement in the nanotunex causing increase in size of the pores and pore throats, related to the process leading to pore size and connectivity increment in actual reservoir.

As the reservoir responds to the combined effect of changes in pore pressure and stress states, the bulk volume will adjust (Geertsma, 1957), changing the pore geometry and connectivity as described above and dependent parameters like porosity, absolute permeability, effective permeability, phase saturations, capillary pressure and transmissibility (Li & Chalaturnyk, 2004). The interaction of these parameters and the dynamic effects of production and/or injection lead to changes both within the reservoir and within the surrounding rock mass. It is important to emphasize, rock properties that control pore geometry and connectivity also affect fluid movement and fluid distribution in the reservoir and the geomechanical modifications of these rock properties will affect flow patterns and ultimately the recovery (Settari, 2002; Rodrigues et al., 2007).

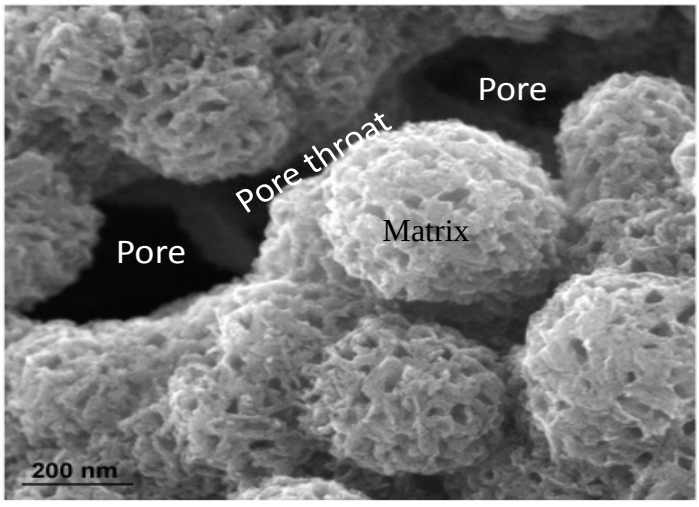

Figure 1.1: SEM micrograph of high surface area Nanotunex (original image adapted from y-carbon.us)

The common approach to modeling fluid movement and distribution in the reservoirs is the use of phase permeability and saturations through the relative permeability functions to account for the interactions between fluids and the porous media. It is quite surprising that relative permeability has received so little attention as a coupling parameter in reservoir-geomechanical simulations considering the volume of literature devoted to this subject over the last decade (Settari and Mourits, 1998; Tortike and Farouq, 1992; Longuemare et al., 2002; Minkoff et al., 2004; Dean et al., 2003; Rodrigues, 2009). The results of laboratory experiments reported in the literature (Ali et al., 1987, Oldakowski, 1994; Wilson, 1956; Jones et al. 2001; Khan 2009 and Hamoud et al., 2012); and summarized in section 2.3 below, support the proposition that geomechanical processes can influence relative permeability functions but these effects have yet to be incorporated into coupled reservoir geomechanical simulations.

1.3 Objective of the Research

The primary target of this study is the coupling of stress dependent relative permeability and reservoir simulation to examine how geomechanically-influenced relative permeability may impact flow. An equally significant aspect of this work is the identification of trends in changes of relative permeability and saturation end point values as the in-situ stress changes, and development of prediction equations for simulation studies.

Coupled models which incorporate not only the change in permeability and porosity but also the changes in relative permeability can lead to more realistic

production forecast especially for reservoirs under improved or enhanced oil recovery scheme as found in heavy oil and oil sands projects.

1.4 Scope Statement

This project will require performing reservoir-geomechanical simulation with porosity, permeability and relative permeability modification as stress changes. Empirical relationship relating porosity, permeability and geomechanics exist in the literature while none exist in-case of relative permeability. Although, this thesis is not an experimental thesis, however, the prediction equation for stress dependent relative permeability was developed from existing experimental data to achieve the target objective.

1.5 Methodology

The following steps are taken to achieve the coupling of stress dependent relative permeability and reservoir simulation:

1. Quality assurance and synthesis of triaxial compression and radial extension experimental test data;
2. Identification of trends in changes of relative permeability and saturation end point values as the in-situ stress changes and development of stress-dependent relative permeability functions;
3. Construction of grids:
    - reservoir simulation grid; and
    - mechanical earth model for geomechanics;
4. Development of the coupling module between the reservoir simulator and geomechanical code;

5. Creation of multiple relative permeability tables that match the number of grid blocks in the simulation model; and
6. Execution of uncoupled and coupled simulation

Chapter 2

Literature Review

2.1 Reservoir Simulation Overview

The huge investments required for field development justify the need for management to base decisions on the fullest technical appraisals that are possible within the narrow time frame (Archer et al., 1975). Reservoir simulation has been used extensively in this regards, in planning the optimum exploitation of virgin fields, as well, re-development of brown fields and to evaluate the effects on recovery of altered operating conditions, in addition, to compare economics of different recovery methods (Coats, 1987).

It is applied in all operations, irrespective of the recovery mechanism, to estimate performance and also to reach decision concerning enhanced oil recovery options, well counts and spacing (Coats, 1968). In addition, optimum horizontal well length, steam injection rate, tracking of the movement of fluid and in combination with analytical solutions to solve major production impairment issues.

2.1.1 Defining a Reservoir Model

Reservoir models are characterized by the static reservoir description and the dynamics of multiphase flow. The reservoir description is mainly the volumetrics and the architecture, while the dynamics of the multiphase flow is defined through the relative permeability and capillary pressure. The scope and

purpose of the reservoir studies dictate the kind and size of model that could be used. The various classes of model include: full-field models, segment models, cross-sectional models and single-well models (Hillestad, 1986).

Reservoir grids are constructed with related boundary conditions included to represent reservoir fluid flow from grid block to grid block in one, two, or three dimensions and consequently termed one-dimensional, two-dimensional, or three-dimensional models. Each grid block is assigned its specific reservoir properties of size, porosity, permeability, elevation, pressure, and fluid saturations (Staggs and Herbeck, 1971; Aziz and Settari, 1979).

In addition to grid block properties, well data are also provided. These include location, rates, and production constraint such as economic limit, maximum water cut and gas-oil ratio (GOR), and minimum bottom-hole flowing pressure. General fluid and rock data is also provided for the entire field or section of field being studied. These usually include PVT data for the oil, gas, and water; rock compressibility and relative permeability for each flowing phase (Staggs and Herbeck, 1971).

After populating the grid with the necessary data, a set of mathematical equations are employed to calculate the flow between grid blocks and the fluid saturation and volumes in each grid block. The equations are derived from the continuity equation or mass balance, Darcy's law of flow through porous media, and equation of state. Finite-difference methods are used to solve the model equations, (Staggs and Herbeck, 1971). Finite element methods are equally used.

2.2 Fluid Movement and Distribution in Reservoir Models

The key to good results from a multi-grid blocks model study is good data, relative permeability relationship being one of the most critical. Relative permeability is of extreme importance during reservoir simulation studies due to their ability to predict the movement of water and free gas relative to oil. They establish, for a given phase, a functional dependence between phase saturation and the rocks ability to produce it. Other areas of application include material balance, frontal advance calculations and inflow performance computations.

Absolute permeability is used when describing the flow of a single fluid through a porous rock, while effective and relative permeabilities are employed in multiphase flow. When two or more fluids flow at the same time, the relative permeability (k_{ri}) of each phase at a specific saturation is the ratio of the effective permeability (k_r) of the phase to the absolute permeability (k) (Tarek et al., 2001).

$$k_{ri} = \frac{k_r}{k} \quad \text{.....2.0}$$

The relative permeability relationship is non-linear, and can be approximated by Equation 2.1 below (Honarpour et al., 1986).

$$k_{rw} = A(S_w)^n; k_{ro} = B(1 - S_w)^m \quad \text{.....2.1}$$

where; A, B, n and m are constants.

2.2.1 Measurement of Relative permeability

Laboratory methods available for measuring relative permeability are: steady state, unsteady-state, capillary pressure methods, centrifuge methods and calculation from field data. The two most widely used methods are the steady state and the unsteady-state methods (Honarpour et al., 1986).

In the steady state method, a fixed ratio of fluids is forced through the test sample until saturation and pressure equilibrium are established (Honarpour et al., 1986). The steady-state methods are inherently time-consuming because equilibrium attainment may require several hours or days at each saturation level. In addition, these methods require independent measurement of fluid saturations in the core. Their advantages are greater reliability and the ability to determine relative permeability for a wider range of saturation levels. The method is more intense and costly to carry out, (Honarpour and Mahmood, 1988). The steady-state methods include the penn-state method, single-sample dynamic method, stationary fluid method, Hassler method, Hafford method, and dispersed feed method (Honarpour et al., 1986).

The unsteady-state techniques are mostly employed for laboratory measurement of relative permeability, because its measurements can be easily made as compared to the steady-state measurement, although the mathematical analysis procedure is more difficult (Honarpour et al., 1986). Many difficulties are also inherent in the unsteady-state methods. Operational problems such as capillary end effects, viscous fingering, and channeling in heterogeneous cores are difficult to monitor and to account for properly. The main advantages of these

methods include fewer instrumentation requirements and substantially reduced test times compared with steady-state tests (Honarpour and Mahmood, 1988).

2.2.2 Two-Phase Relative Permeability Model

Presently, there are four categories of mathematical models for describing relative permeability curves: capillary model, statistical model, empirical model and network model. Empirical models are becoming more popular, particularly with the advent of reservoir simulators (Esteban et al., 2003).

Today several two-phase empirical relative permeability models that relate the end point saturations to produce the relative permeability curve exist. But, the Modified Brooks and Corey models (MBC) in the form of power law, shown in Equations 2.13 and 2.14 below, are mostly utilized by the petroleum industry in numerical simulators (Tarek et al., 2001).

- Water Relative Permeability

$$k_{rw} = k_{rw}^{'}\left(S_{wn}\right)^{n_w} = k_{rw}^{'}\left(\frac{S_w - S_{wi}}{1 - S_{wi} - S_{or}}\right)^{nw} \quad \text{.....2.13}$$

- Oil Relative Permeability

$$k_{ro} = k_{ro}^{'}\left(S_{on}\right)^{n_o} = k_{ro}^{'}\left(\frac{1 - S_w - S_{or}}{1 - S_{wi} - S_{or}}\right)^{n_o} \quad \text{.....2.14}$$

2.3 Stress Dependent Relative Permeability

Morgan and Gordon (1970) discussed extensively on the relationship between relative permeability and saturation end points and the pore geometry.

They described that rocks with large pores and correspondingly small surface areas have low irreducible water saturations that leave a relatively large amount of pore space available for the flow of fluids. This condition allows high end point permeabilities to exist and allows a large saturation change to occur during two phase flow. On the other hand, rocks with small pores have larger surface area and irreducible water saturations that leave little room for the flow of fluids. This condition causes low end point relative permeability to oil and water values.

Wilson (1956), measured steady state oil-water relative permeability for rock samples subjected to different pore pressures up to 35 MPa and overburden pressures up to 69 MPa. Wilson found that increasing the overburden pressure caused a reduction in oil and water effective permeabilities in about the same proportion as it affects the single-phase (absolute) permeability.

Ali et al. (1987), conducted unsteady state experiments on Berea sandstone cores with net hydrostatic overburden pressure in the range 0.69 - 41.37 MPa, and observed a decrease in oil relative permeability and negligible effects in brine relative permeability with increase in applied pressure. It was also noted that there was an increase in end point saturations with increasing stress.

Oldakowski (1994) performed experiments to measure the water effective permeability of oil sand samples over a range of stress paths and observed an increase in effective permeability to water when the confining stress was reduced from 6 MPa to 0.1 MPa. It was concluded that water effective permeability can be significantly increased by shear induced volume changes or dilation.

Jones et al. (2001) also measured the stress sensitivity of relative permeability in a number of sandstones and showed that end-point effective permeability was more stress sensitive than absolute permeability. The end point saturations were equally observed to be stress sensitive.

Perhaps the most definitive work to date was testing conducted by Khan (2009) who performed triaxial compression and radial extension test on different Ottawa sand samples and observed that end point relative permeability increased during dilation and decreased during compression. The residual oil saturation was found to increase during compression and decreased during dilation. While, the irreducible water saturation initially decreased and later increased as axial load was increased for triaxial compression test at 345 kPa confining pressure. However, the irreducible water saturation was reported to increase throughout for test performed at 1379 kPa confining stress. Meanwhile, for the radial extension test, the irreducible water saturation was observed to initially increase up to a peak value and slightly decrease as the effective stress was further decreased.

Hamoud et al. (2012) have recently completed a reservoir-geomechanical testing program to explore primarily how shear induced volume changes impact residual oil saturation, initial oil saturation and oil-water relative permeability curves in a dense reconstituted sand specimen. While these results confirmed similar irreducible water saturation variations during compression and dilation, the residual oil saturation displayed complex behavior related to the shear induced volumetric strains within the specimens.

2.4 Reservoir Geomechanics

Geomechanics is generally employed in characterizing stress, strain and deformation in subsurface operations. Stress is a concept which is fundamental to geomechanical principles and applications**.** There are three basic reasons to understand stress in subsurface operations. First, for the purpose of engineering analysis and design, there is the need to understand the pre-existing stress state associated with geologic setting in the subsurface. Secondly, engineering activities, like production or injection, can dramatically change this stress state and lastly, stress is a tensor quantity and tensors are not encountered in everyday life, (Hudson and Harrison, 1997).

Terzaghi's theory of effective stress and Biot's generalized 3D theory of consolidation are the basics of geomechanics. The coupling of deformation and fluid-flow problem was first analyzed by Terzaghi in 1925 as a consolidation problem. All the measurable effects of a change of stress, such as compression, distortion and change in shearing resistance are exclusively due to changes in effective stress. Since then Terzaghi's 1D consolidation theory has been used widely. Biot extended the theory into a more general 3D case, to account for compressibility of both fluid and solid component, (Gutierrez et al., 2001). However, Geertsma (1957) argued that the Biot's formulation introduced a number of deformation constants which are impractical for reservoir rocks from an experimental determination perspective and proposed a theory that requires only three elastic constants and three viscous constants for describing pore and rock bulk volume variations. Geertsma's theory enables the Biot's constant to be

expressed in terms of compressibility and porosity.

Skempton (1960) also derived a relationship between the total stress and fluid pore pressure which considers compressible particle but incompressible pore fluid. Ghaboussi and Wilson (1973) introduced fluid compressibility into classic soil mechanics consolidation theory. Also, Rice and Cleary (1976) showed how to solve the poro-elastic problems by assuming pore pressure and stress as primary variables instead of displacements as employed by Biot (Jalali and Dusseault, 2008).

2.5 Coupling Flow and Geomechanics

Standard reservoir simulator conventionally considers porosity, permeability, constant rock compressibility, fluid movement, pressure changes and production history in its calculation, while rock deformation with reservoir disturbance is ignored. Reservoir simulator mainly uses the constant pore compressibility to account for the pressure changes due to volumetric changes in the rock (Stone et al., 2000), ignoring bulk medium movement that accompanies rock expansion and contraction (Tran et al., 2005). This simplifying assumption is not sufficient to reproduce pore volume changes induced by complex pressure and temperature variations (Settari and Mourits, 1998; Tortike and Farouq, 1993).

An understanding of the dynamic changes within the reservoir and its surrounding is important because of issues like production-induced compaction and subsidence, well and completion integrity, cap-rock and fault-seal integrity, fracture behavior, pore collapse as well as loss and gain in production, (Gutierrez

and Lewis, 1998; Settari and Mourits, 1998). Reservoir simulator alone cannot model these phenomena, since it does not incorporate stress changes and rock deformations due to changes in reservoir pressure and temperature, (Tran et al., 2005). For these kinds of field issues, in-situ stresses and rock deformations, in addition to flow behavior are key parameters in controlling the recovery response (Gutierrez and Lewis, 1998).

Early work in coupling of flow and geomechanics used the concept of pore compressibility to model the response of the skeleton of a porous medium to fluid flow (Settari and Mourits, 1998). According to Tortike and Farouq (1991), this coupling approach suffers numerical instabilities problems which may propagate and interfere with the pressure solution. They proposed an explicit coupling scheme in which the coupling terms are supplied externally to each of the component models.

Gutierrez and Lewis (1998) used the extension of Biot's theory proposed by Lewis and Sukirman (1993) to demonstrate that fluid flow and reservoir deformation are fully-coupled processes, and that such coupled behavior cannot be sufficiently represented by a pore compressibility parameter as is done in reservoir simulators. Each of these positions clearly showed that the deformations resulting from pore volume change cannot be modeled without obeying fundamental law of stress equilibrium and without honoring the displacement boundary conditions along the contact between the reservoir rock and the adjacent rocks (Inoue et al., 2009). The interaction between stress,

pressure and flow in a porous medium requires effective coupling between geomechanics and reservoir flow.

2.5.1 Coupling Approach

There are several ways to achieve the coupling between flow and geomechanics and today different techniques exist for implementing geomechanical effects into reservoir simulation. They are: classical, one-way coupling, pseudo coupling, sequentially coupled and fully coupled approach (Tortike and Farouq, 1992; Longuemare et al., 2002; Minkoff et al., 2003; Dean et al., 2003; Rodrigues, 2009). They differ on accuracy, adaptability, running speed, elements of geomechanics implemented and the degree to which these elements are coupled to multiphase fluid flow (Samier et al., 2003; Gutierrez et al., 2001; Trans et al., 2009; Settari and Walter, 1999).

2.5.1.1 Classical Approach

In this technique, the numerical simulator only is used. The nonlinear, time dependent, mass behavior of the rock matrix is ignored. Variation of the pore volume is considered simply through the rock compressible, which is a constant value in the simulator.

2.5.1.2 One Way Coupling

As the name implies, pressures calculated by the reservoir simulator is introduced as an external load to the geomechanical code to compute new stress

and strain, (Settari and Walter, 2001); however, the results are not used in updating the reservoir properties, they are only used in accessing the stress and strain variation. This coupling approach is easy to implement and still includes some interesting physics (Longuemare et al., 2002).

2.5.1.3 Pseudo Coupling

This approach is very similar to porosity and permeability adjustment in conventional flow simulation history match. As explained by Rodrigues (2009), the technique uses the permeability and porosity multipliers approach, where the impact of geomechanics is translated to the flow simulation run by multiplication factors calibrated from laboratory and field data. The flow simulator alone is used, but it carries out the geomechanical computation at time zero to investigate if the reservoir is sensitive to geomechanics parameters.

2.5.1.4 Sequentially Coupled

In this scheme, the pressures calculated by the flow simulator are sent to the geomechanical code for stress and strain calculation and the results used in updating porosity and permeability for pressure calculation for the next time step, (Settari and Walter, 1999; Dean et al., 2003; Longuemare et al., 2002; Minkoff et al., 2003). Both the flow and geomechanical simulator at run time share information in both directions through an interface code unlike the one way coupling. This approach produces the same results as the fully coupled, if both techniques use sufficiently tight convergence tolerances for iterations (Dean et al.,

2003). The primary attraction is that it is very straightforward to couple a commercial simulator with an existing geomechanics code (Minkoff et al., 2003).

2.5.1.5 Fully Coupled

The flow variables (pressure and temperature) and geomechanical variables (stress, strain and displacement) are solved simultaneously through a system of equations in the case of the fully coupled manner (Trans et al., 2009). Problems associated with implementation of the fully coupled approach are the difficulties in coupling existing flow simulator and geomechanics code, intensive code development than other techniques and the run time (Dean et al., 2003).

2.5.2 Coupling Parameters

There are two main components of the coupling between fluid-flow and geomechanics (Settari and Mourits, 1998). The two components are; coupling through volume and coupling through flow properties.

2.5.2.1 Volume Coupling

The main quantities required in order to predict fluid movement and productivity in a reservoir are the fluid pressures. When the rock deformation affects fluid pressure and vice versa, the volume coupling is considered (Gutierrez et al., 1998). The volume change calculated by the geomechanical code is more accurate because it is calculated directly from volumetric strain of the porous media based on the material constitutive model (Settari and Mourits, 1998).

2.5.2.2 Coupling through Flow Properties

The other coupling approach, coupling through flow properties, is used when the change in pore structure due to rock deformation will affect permeability and relative permeability (Gutierrez et al., 1998).

Chapter 3

Methodology

Phase distribution and movement are important processes in understanding the dynamics of multiphase flow in reservoir studies. Distribution and movement of a set of reservoir fluids depends on the rock-fluid system defined by the relative permeability relationship. As illustrated in section 1.2, changes in pore geometry due to the alterations in in-situ stress affect this flow function. Hence modeling of the dynamics of multiphase flow in recovery processes requires effective coupling between flow simulator and geomechanics code. In this work, IMEX^{TM} and FLAC3D^{TM} were linked through an interface code written in Visual Basic (VB) to investigate the impacts of stress dependent relative permeability on flow.

3.1 Application of IMEX^{TM}

IMEX^{TM} is a black oil simulator built by the Computer Modeling Group (CMG) Limited. It has the capability of modeling the flow of three phase fluids in gas, gas-water, oil-water, and oil-water-gas reservoirs. It can support modeling up to three dimensions, including multiple PVT and equilibrium regions as well as multiple rock types and flexible relative permeability choices (CMG, 2008).

The governing equations for the black oil simulator are non-linear partial differential equation (Equations 3.1, 3.2 and 3.3) and as a result of gridding and finite differencing these equations are replaced with a set of nonlinear algebraic equations. IMEX^{TM} solves these set of equations, calculating pressure and

saturation in each grid blocks at each time step. The adaptive implicit formulation is used in this study.

$$\nabla \cdot \left[\lambda_o \left(\nabla p_o - \gamma_o \nabla_Z\right)\right] = \frac{\partial}{\partial t}\left[\frac{\phi S_o}{B_o}\right] + q_o \quad \text{.....3.1}$$

$$\nabla \cdot \left[\lambda_w \left(\nabla p_w - \gamma_w \nabla_Z\right)\right] = \frac{\partial}{\partial t}\left[\frac{\phi S_w}{B_w}\right] + q_w \quad \text{.....3.2}$$

$$\nabla \cdot \left[R_s \lambda_o \left(\nabla p_o - \gamma_o \nabla_Z\right) + \lambda_g \left(\nabla p_g - \gamma_g \nabla_Z\right)\right] = \frac{\partial}{\partial t}\left[\phi\left(\frac{R_s}{B_o} S_o + \frac{S_g}{B_g}\right)\right] + R_s q_o + q_g \quad \text{..3.3}$$

$$\lambda_l = \frac{k_{rl}}{\mu_l B_l} k \quad \text{.....3.4}$$

Equations 3.1, 3.2 and 3.3 contain six dependent variables. Three additional relations, Equations 3.5, 3.6 and 3.7 are used to complete the description, (Aziz, 1979).

$$S_o + S_w + S_g = 1 \quad \text{.....3.5}$$

$$P_{cow} = P_o - P_w = f\left(S_w, S_g\right) \quad \text{.....3.6}$$

$$P_{cog} = P_g - P_o = f\left(S_w, S_g\right) \quad \text{.....3.7}$$

3.2 Application of FLAC3D™

Fast Lagrangian Analysis of Continua in 3-Dimensions (FLAC3D) is a three-dimensional explicit finite-difference program for engineering mechanics calculations. The code was created by Itasca Consulting Group. During computations, each grid blocks in a model is constrained to behave according to a

prescribed linear or nonlinear stress/strain law in response to applied forces or boundary restraints (Itasca Consulting Group, 2011).

FLAC3D^{TM} determines the motion of an elementary volume of the medium from the forces applied to it. The Cauchy's equation of motion (Equation 3.8) is solved to compute the translational velocity $[\upsilon]$ in the grid, while the corresponding component of the strain-rate tensor is calculated using Equation 3.9 from which the strain is computed (Itasca Consulting Group, 2011). The constitutive equation that defines the nature of the reservoir's material (Equation 3.10) is then solved to generate the stress increments. In this work, the linear elastic constitutive equation was used in predicting the failure conditions of the grid when the initial stress condition is altered. The new stress values are calculated from Equation 3.12

$$\sigma_{ij,j} + \rho b_i = \rho \frac{d v_i}{dt} \quad \text{.....3.8}$$

$$\xi_{i,j} = \frac{1}{2}\left(\upsilon_{i,j} + \upsilon_{j,i}\right) \quad \text{.....3.9}$$

$$\bar{\sigma} = \Psi_{ij}\left(\sigma_{ij}, \xi_{ij}, \kappa\right) \quad \text{.....3.10}$$

The boundary and initial stress conditions are defined and appropriate check made to ensured that no displacement occur at zero time in the grid. Following the computational method in FLAC3D^{TM}, effective stresses are used; the pore pressures are applied to convert total stresses (Equation 3.11) to effective stresses before using the constitutive model. The reverse occurs after the model

calculations are completed. Compressive stress and strain are taken as negative (-), while the tensile stress and strain values are taken as positive (+).

$$\sigma_{i,j}{}' = \sigma_{i,j} + I\alpha p \quad \text{.....3.11}$$

$$\sigma^{N}_{i,j} = \sigma_{i,j} + \Delta\sigma_{ij} \quad \text{.....3.12}$$

3.3 Coupling IMEX^{TM} and FLAC3D^{TM}

The sequentially coupled approach was used in this work to couple IMEX and FLAC3D to perform the coupled simulation, using procedures implemented by various researchers **(**Li and R.J. Chalaturnyk, 2006; L. Rodrigues, 2009; R. Rodríguez, 2010; and Minkoff et al., 2004). As explained in section 2.5.1.4, the approach allows IMEX and FLAC3D to exchange information through a third party code in both directions.

Figure 3.1 illustrates the simulation process diagram. Pressures calculated by IMEX in each of the grid blocks are written to an excel spreadsheets and used by FLAC3D for the calculation of new stress and strain values. After the geomechanics solution is obtained, strain values are used by the code to update porosity and permeability. The new porosity values are used in updating relative permeability and saturation endpoint values that are in-turn used in adjusting the relative permeability tables. The updated values are written to an assigned spreadsheet and applied by IMEX for new pressure calculation. The process of coupling is repeated until the end of the final time-steps assuming there were no convergence issues. The coupling approach is an explicit one in the sense that

pressure is calculated using permeability, porosity, and relative permeability values updated with geomechanics calculations performed at the previous time step.

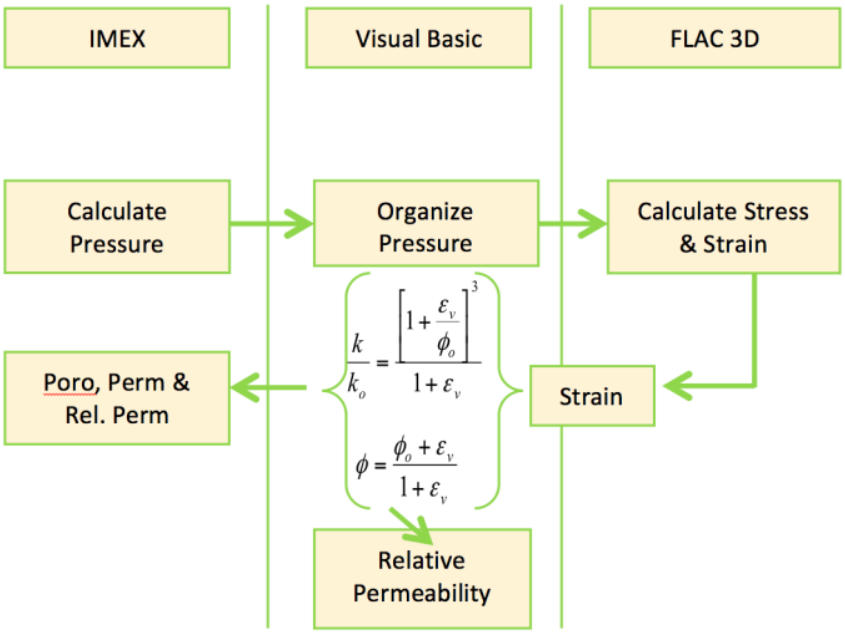

Figure 3.1: Iterative coupled simulation process

3.4 The Coupling Module

The code used in coupling IMEX and FLAC3D was created by the Reservoir Geomechanics Research Group $(RG)^2$ at the University of Alberta using the visual basic programming language in Microsoft Excel. Simulation control (Figure 3.1), automatic entering and organization of data, as well as manual data input are done via different excel sheets. Each spreadsheet was programmed to perform a specific task. As shown in Figure 3.2, the reservoir grid location in the MEM can be specified and varied using the simulation control spreadsheet.

The code calls the flow model and Mechanical Earth Model (MEM) grid files in ".DAT" format and write the grids and properties to various spreadsheets in a format that is readable to IMEX `and FLAC3D. During initialization, IMEX and FLA3D explicitly used the spreadsheets assigned to them to create the flow and geomechanical models.

Also, when performing coupled simulation, the code restrains IMEX and FLAC3D to calculation one after the other at each time step. It organizes pressures for FLAC3D usage; calculates, organizes and updates porosity, permeability and relative permeability functions. The code subsequently uses the MBC's functions (Equations 2.13 and 2.14) to update the relative permeability table. One of the main benefits of the code is the ability to automatically create and update the relative permeability tables at each time step for each of the grid blocks within a short time (about 1 minute).

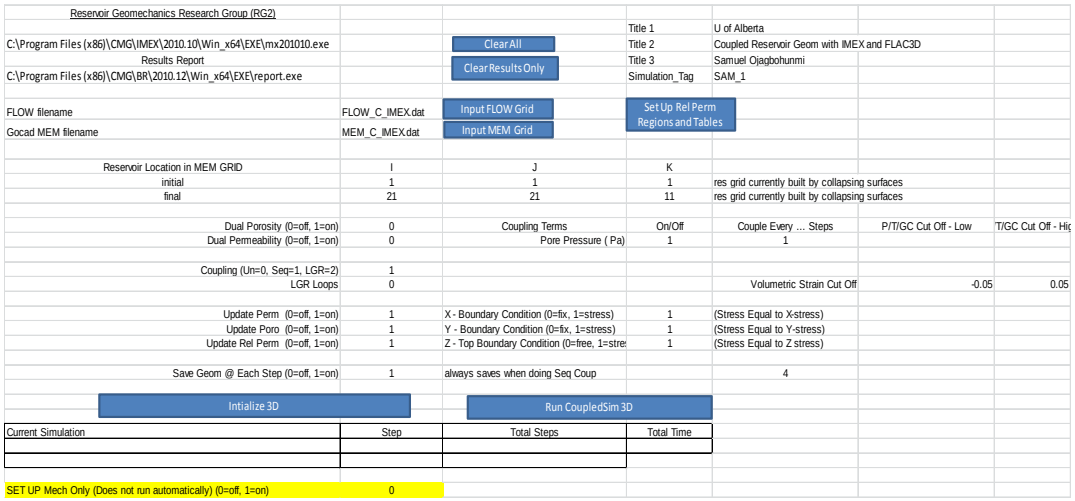

Figure 3.2: Simulation control spreadsheet.

Reservoir Location in MEM GRID	I	J	K
initial	1	1	1
final	21	21	11

Figure 3.3: Reservoir Location in MEM.

3.5 Updating Porosity and Permeability

Equations relating porosity and permeability with volumetric strain proposed by Tortike and Farouq (1993) were used (Equations 3.13 and 3.14) in updating porosity and permeability when the model experienced changes in stress. The volumetric strain contained in the equation is calculated from the axial strain computed by FLAC3D using Equation 3.15.

$$\phi = \frac{\phi_o + \varepsilon_v}{1 + \varepsilon_v} \quad \text{.....3.13}$$

$$\frac{k}{k_o} = \frac{\left[1 + \frac{\varepsilon_v}{\phi_o}\right]^3}{1 + \varepsilon_v} \quad \text{.....3.14}$$

$$\varepsilon_v = \varepsilon_{xx} + \varepsilon_{yy} + \varepsilon_{zz} \quad \text{.....3.15}$$

3.6 Updating Relative Permeability and Saturation End Point

The MBC's model or the power law model, as shown in Equation 2.13 and 2.14, respectively, were applied in generating the relative permeability tables during initialization inside the code written to couple the reservoir simulator and the geomechanical code. The benefit of the MBC model is that it allows new values for any of the relative permeability curve end points to be defined and

updated at every time step. However, theoretical and empirical functions relating geomechanics and relative permeability functions do not exist like in the case of porosity and absolute permeability; therefore empirical functions relating porosity multiplier and relative permeability and saturation end points were generated from triaxial compression and radial extension test data (see Khan (2009) for detail). The analysis of the data is discussed in next section, while the full data used is shown in Appendix D.

Changes to the Corey's water and oil saturation exponent as a function of change in in-situ stress condition were not incorporated into this work. While it is believed that these parameters could be affected by changes in in-situ stress condition, the degree of such effect could not be quantified for lack of data. However, these parameters were considered in the methodology and included in the code written to coupled IMEX and FLAC3D for a future work.

3.6.1 Endpoint Functions

The data used in obtaining the stress dependent relative permeability end point was acquired from Khan's (2009) work. The reader should refer to it for full detail on the data and how they were obtained. The dependent variables (relative permeability and saturation endpoint values) were normalized using Equations 3.16, 3.17, 3.18 and 3.19. The current porosity after the change in the initial in-situ stress condition was obtained using Equation 3.13 above, and the porosity multiplier, Poro* (ϕ^*), was calculated from the ratio of the current to initial porosity (Equation 3.20).

$$k_{ro}^{*} = \frac{k_{ro}}{k_{roo}} \quad \text{.....3.16}$$

$$k_{rw}^{*} = \frac{k_{rw}}{k_{rwo}} \quad \text{.....3.17}$$

$$S_{or}^{*} = \frac{S_{or}}{S_{oro}} \quad \text{.....3.18}$$

$$S_{wir}^{*} = \frac{S_{wir}}{S_{wiro}} \quad \text{.....3.19}$$

$$\phi^{*} = \frac{\phi}{\phi_{o}} \quad \text{.....3.20}$$

Endpoint Relative Permeability to Oil: Figure 3.4 is the plot of the normalised $k_{ro}(S_{wir})$ and the porosity multiplier. The Lower Amalgamated Ottawa and the Lower Fine Ottawa (at 1,379 kPa) data (Khan, 2009) were used in generating this plot, as well as the plots for the endpoint saturation values and relative permeability to water. The coefficient of determination (R^2) for the regression equation is 0.8149, indicating there is a good correlation between the two parameters. The equation for predicting stress dependent relative permeability to oil at irreducible water saturation was obtained from the regression equation as shown below:

$$k_{ro}^{*} = 2.3578\phi^{*} - 1.3962 \quad \text{.....3.21}$$

$$k_{ro} = k_{ro(\varepsilon_v=0)}\left(2.3578\phi^{*} - 1.3962\right) \quad \text{.....3.22}$$

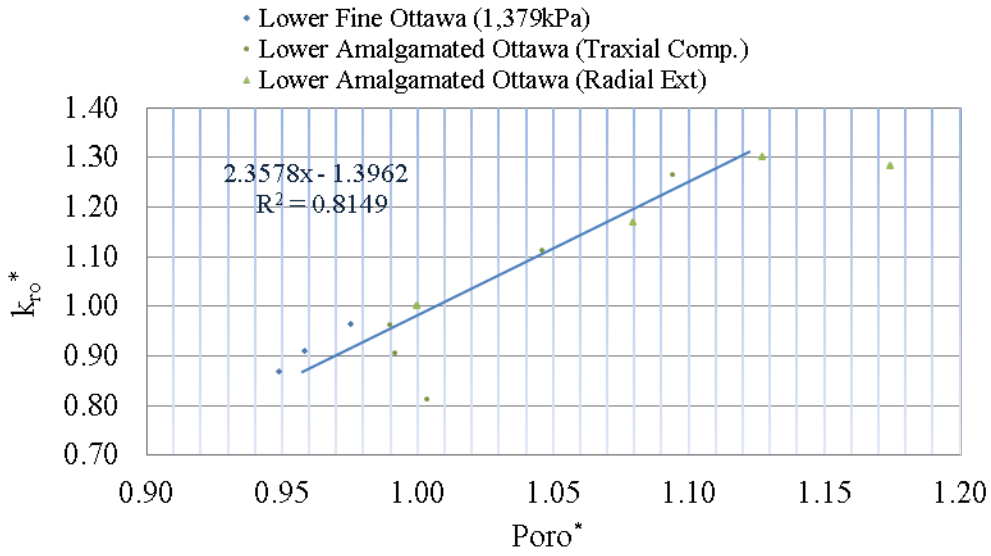

Figure 3.4: Normalised end point k_{ro} vs. porosity multiplier

Validation: The suitability of Equation 3.22 for predicting unknown $k_{ro}(S_{wir})$ values was validated using the data from the Medium Ottawa sample (Khan, 2009). The following values were used:

Porosity = 0.3170

Porosity at 4. 46% increase in volumetric Strain = 0.3462

Porosity multiplier = 1.092

$k_{ro}(S_{wir})$ at initial in-situ stress = 0.55

The value of $k_{ro}(S_{wir})$ increased from 0.55 to 0.648, using Equation 3.22, a value close to 0.64 obtained from the laboratory experiment (Khan, 2009) .

Endpoint Relative Permeability to Water: Similarly, the normalised $k_{rw}(S_{or})$ was plotted against the porosity multiplier (Figure 3.5). There is a good correlation between the dependent and the independent parameters going by the R^2 of 0.8986 from the regression line. The $k_{rw}(S_{or})$ as the stress changes from in-situ condition was also obtained from the regression equation as shown in Equation 3.24.

$$k_{rw}^{*} = 4.3341\phi^{*} + 3.4537 \quad \text{.....3.23}$$

$$k_{rw} = k_{rw(\varepsilon_v=0)}\left(4.334\phi^{*} - 3.454\right) \quad \text{.....3.24}$$

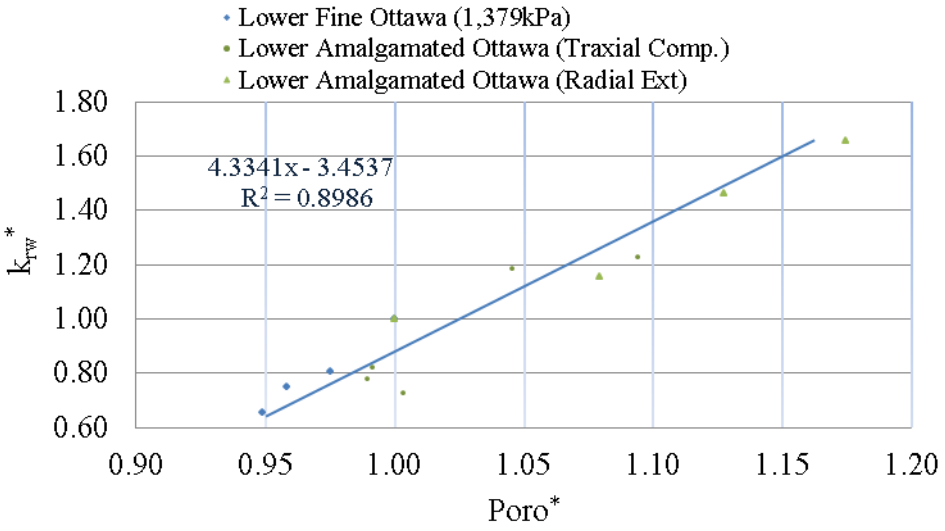

Figure 3.5: Normalised end point k_{rw} vs. porosity multiplier

Validation: Like in the previous case, the suitability of the $k_{rw}(S_{or})$ function was equally validated using the same data as above and initial in-situ $k_{rw}(S_{or})$ of 0.17.

The $k_{rw}(S_{or})$ will increase from 0.17 to 0.21, using Equation 3.24, a value close to 0.19 obtained from the experimental data.

Residual Oil Saturation: Similar to the case of the relative permeabilities, the S_{or}^{*} also displayed some good correlation with the porosity multiplier as shown in Figure 3.6, going by the R^2 of 0.8086 obtained from the regression line. The S_{or} model was obtained from the regression equation as shown below:

$$S_{or}^{*} = 5.2527 - 4.1089\phi^{*} \quad \text{.....3.25}$$

$$S_{or} = S_{or(\varepsilon_v=0)}\left(5.2527 - 4.1089\phi^{*}\right) \quad \text{.....3.26}$$

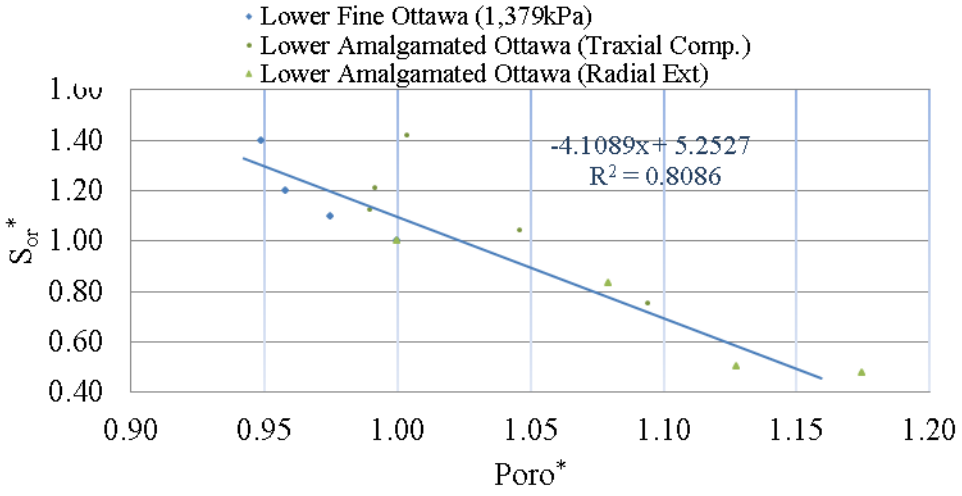

Figure 3.6: Normalised residual oil saturation vs. porosity multiplier

Validation: The function obtained above was validated using the same data used in the $k_{ro}(S_{wir})$ with initial in-situ S_{or} of 0.26. With Equation 3.26, the S_{or} will decrease from 0.26 to 0.20 when the pore volume increased by 4.46%. The predicted value is very close to 0.22 obtained by Khan (2009).

Irreducible Water Saturation: Because the data points in Figure 3.7 did not show a singular well defined trend between the paths of increasing and decreasing stress, the regression equations for volumetric compression and dilation induced data were obtained separately. The S_{wir} function for compression was obtained from the trend line drawn through the Lower Fine Ottawa sample at 1379 kPa confining stress (Figure 3.7). While, the S_{wir} function for dilation (polynomial regression type) was obtained using the regression line through the Lower Amalgamated data. The functions were obtained as follow:

1) Irreducible water saturation during compaction:

$$S_{wir}^{*} = 7.9525 - 6.9857\phi^{*} \quad \text{.....3.27}$$

$$S_{wir} = S_{wir(\varepsilon_v=0)}\left(7.9525 - 6.9857\phi^{*}\right) \quad \text{.....3.28}$$

2) Irreducible water saturation during dilation:

$$S_{wir}^{*} = -35.15\phi^{*2} + 76.72\phi^{*} - 40.56 \quad \text{.....3.29}$$

$$S_{wir} = S_{wir(\varepsilon_v=0)}\left(-35.15\phi^{*2} + 76.72\phi^{*} - 40.56\right) \quad \text{.....3.30}$$

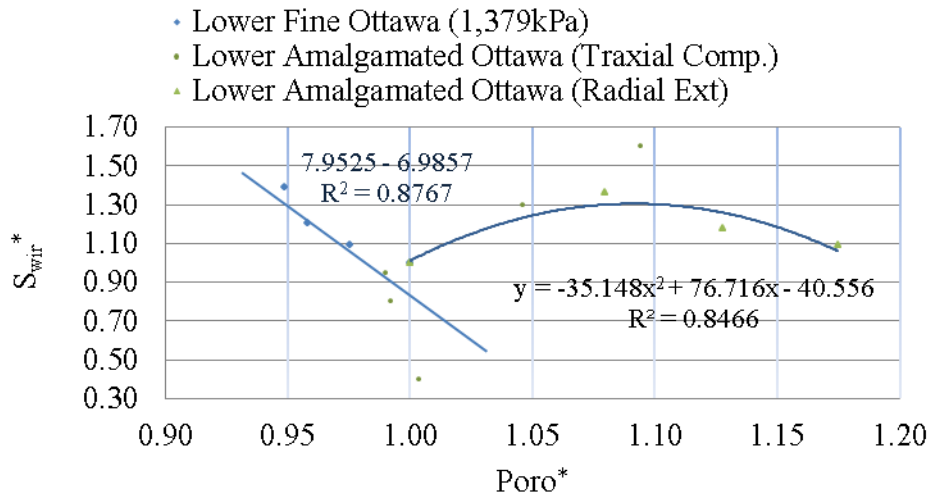

Figure 3.7: Normalised irreducible water saturation vs. porosity multiplier

Validation: The S_{wir} model for dilation was equally validated using the same data as before, S_{wir} of 0.10 was applied. The S_{wir} increased from 0.10 to 0.13, which is exactly what was obtained from the experimental data (Khan, 2009).

3.6.2 Geomechanical Shift in the Relative Permeability Curve

The shift in the relative permeability curve for a stress sensitive reservoir can be with illustrated using Figure 3.8 for two different porosity multiplier values, 0.9882 and 1.0417 respectively, representing volumetric compression and dilation dominated processes. The following observations can be made about Figure 3.8:

- An increase in the volumetric strain (dilation) shifts the entire k_{ro} curve to the right and causes an increase in the end point k_{ro} from 0.510 to 0.562.
- The neutral point also increased, similar to the case of the effect of wettability alteration on relative permeability in which the neutral point

could be said to have shift towards being more water wet. The neutral point is the point at which the values of k_{rw} and k_{ro} are both equal. The neutral point increased compared to the un-deformed relative permeability curve.

- There was very little or no shift in the relative permeability to water (k_{rw}) curve up to water saturation value of 0.585, but a shift to the right as the water saturation further increased. The end point k_{rw} increased from 0.3906 to 0.4622.
- Volumetric compression caused insignificant changes in both the k_{ro} and the k_{rw} curve. However, the $k_{ro}(S_{or})$ decreased from 0.5102 to 0.4957 while the $k_{rw}(S_{wir})$ from 0.30 to 0.32.
- The neutral point for volumetric compression in this case does not show significant changes.

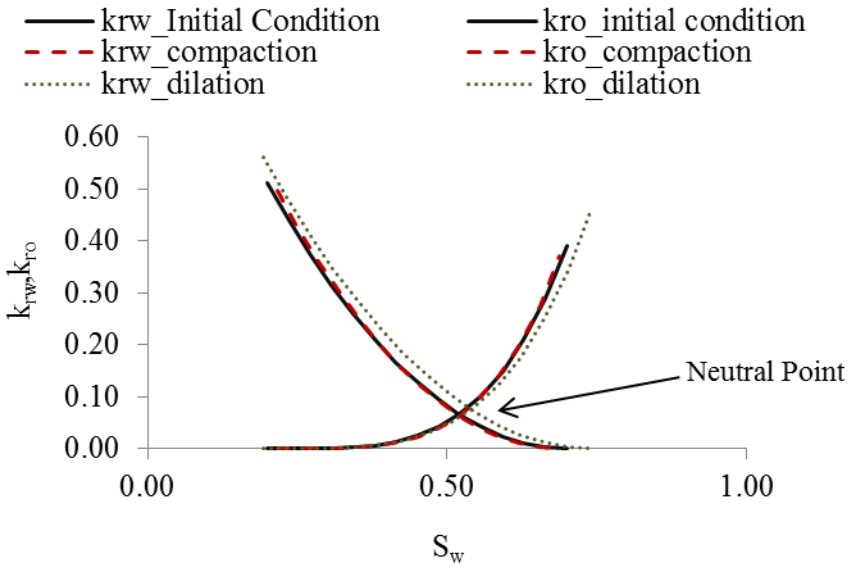

Figure 3.8: Shift in relative permeability curve.

3.7 Model Construction with JewelSuite™

JewelSuite™ (now owned by Baker Hughes Inc.) is a full workflow-integration framework that supports every step needed to build complex reservoir models in 2-Dimention (2D) and 3-Dimension (3D). Fast 2D and 3D viewers are available throughout the whole workflow, allowing you to obtain details on all aspects of the reservoir (JOA, 2009). It has a complete step-by-step workflow methodology which is very interactive.

JewelSuite was used in constructing both the flow grid and the geomechanical grid for the stress analysis, following the workflow shown in Figure 3.9. The gridding and layering were tied to the study objective and the memory usage.

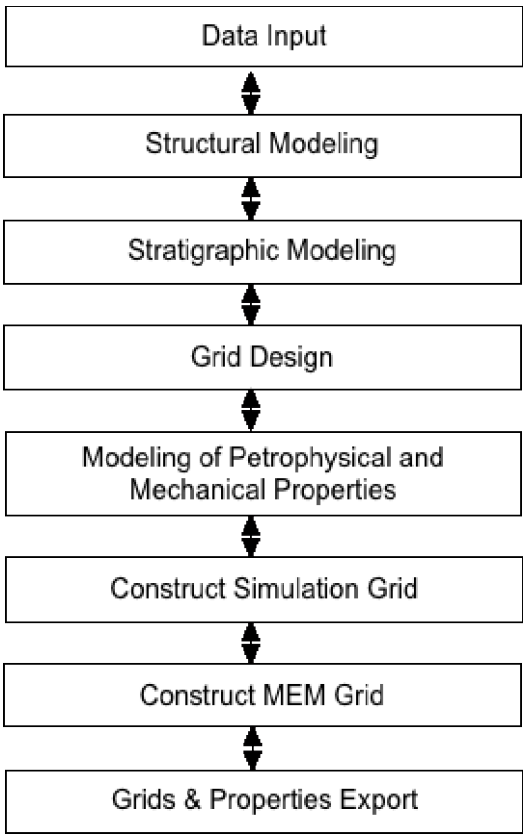

Figure 3.9: Model construction workflow.

3.8 Implementation of the Methodology

The work-flow adopted to implement the methodology aligned strictly with the study objectives. The work steps listed in section 1.4 were followed and each of them is fully enumerated in the subsequent sections.

3.8.1 Reservoir Description

The reservoir description involved integration of the three independent components: 1) fluid properties; 2) rock petrophysical and mechanical properties and; 3) reservoir framework.

3.8.1.1 Fluid Properties

An undersaturated oil system was used in the simulation studies. The pressure volume and temperature (PVT) model used was generated by matching available parameters using standard PVT correlations. The available parameters are the bubble point pressure, oil API gravity, gas gravity and reservoir temperature. The correlations selected are shown in Table 3.1.

Table 3.1: Selection of correlations

Properties	**Selected Correlation**
Oil	
Bubble Point Pressure	Standing
Solution Gas-Oil Ratio	Standing
Formation Volume Factor	Standing
Dead oil Viscosity	Ng and Egbogah
Live oil Viscosity	Beggs and Robison
Oil Compressibility	Glaso
Gas	
Gas Critical Properties	Standing

3.8 Petrophysical Properties Modeling

Rock petrophysical and mechanical properties assigned to the grids were defined by allocating constant values to each layer. The full properties used in populating the model, both the flow model and MEM are shown in Table 3.2.

Table 3.2: Model Properties

Model	**Properties**
Flow Model	Permeabilities (X, Y and K), Porosity, Water Saturation, Oil Saturation
MEM	Vertical and Horizontal Stress values, Poisson's Ratio, Bulk Modulus, Young's Modulus, Shear Modulus and Density,

3.8.1.3 Grids Construction

A simple model was constructed using corner point gridding. This enabled appropriate transmissibility's and pore volume to be calculated. Also, FLAC3D uses a corner-point gridding system, facilitating efficient exchange of information between the two codes. Equal areal dimension (ΔX and ΔY) and vertical thickness were used in the grid design. The stratigraphic layering method was used to divide the reservoir into different layers

The same geologic structure and grid used in the flow grid was used for the MEM. The values of the Young's modulus and Poisson's ratio were used in generating the bulk and shear moduli using Equation 3.48 and 3.49 respectively.

$$K = \frac{E}{3(1-2\nu)} \quad \text{.....3.48}$$

$$G = \frac{E}{2(1+\nu)} \quad \text{.....3.49}$$

3.8.2 Rock-Fluid Properties

Oil-water and liquid-gas relative permeability tables were created for the interblock fluid flow using the MBC's functions (Equations 2.13 and 2.14). The benefit is that it allows new values for any of the end points to be defined and updated. In actual field cases as production progresses, water saturation increases, likewise gas saturation, assuming there was a decline in reservoir pressure. Because of this, the imbibition oil-water and drainage liquid-gas relative permeability curve were used.

Normally, IMEX requires one oil-water relative permeability table and one liquid-gas relative permeability table for each relative permeability regions. However, in this work, relative permeability tables were assignment to each grid block, because of the different response to stress created in different segments of the grid, especially near the production and injection well area.

3.9 Model Initialization

The flow model was initialized and debugged to correct improper data entry, a similar process for any simulation work. Initialization was also a way of representing the zero time where the flow model parameters were set to initial reservoir conditions. It also includes the calculation of initial pore volumes,

pressures and saturations, and original fluids in place.

Likewise, the MEM was made to reach mechanical equilibrium between the applied boundary conditions and the initial state of stress in the grid. This was required before the coupled simulation to ensure that before the creation of the disturbance in the grid, shear stresses and volumetric strains values in each grid block were all zero.

3.10 Validation of Methodology

3.10.1 Uncoupled Simulation

Before validating the sequentially coupled approach, a production forecast was completed on the flow model using IMEX alone (uncoupled simulation). Geomechanical effects were not considered. This established a point of reference or base case for the coupled simulations, as the results are compared with that of the uncoupled simulation. It is equally important at the early stage to validate the influence of geomechanics on the model as the target objective relies heavily on the occurrence of deformation in the model during the simulation.

3.10.2 Coupled_1 Simulation

IMEX and FLAC are coupled at the early stage to ascertain if there was an impact of geomechanics on the production profile. For this simulation case, porosity and permeability are used as the coupling parameters. This is the main approach used so far in the literature (Minkoff et al., 1999; Li and R.J

Chalaturnyk, 2001; Trans et al., 2003; L. Rodrigues, 2009; R. Rodriguez, 2010).

3.10.3 Coupled_2 Simulation

The final simulation case uses porosity, permeability and relative permeability as coupling parameters to investigate the effects of geomechanics on production profile. As in the case of the ‘coupled_1’ simulation above, results from the ‘coupled_2’ simulation were also compared with the results from the uncoupled and ‘coupled_1’ simulation.

Chapter 4

Case Study

4.1 Introduction

Considering the impacts on recoverable reserves, the geomechanical aspect of non-isothermal immiscible displacement is an important problem for the petroleum reservoirs. A non-isothermal immiscible displacement is chosen for this work because of the different stress path experienced by the different grid blocks due to pressure depletion and re-pressurization localization in the entire grid.

The oil produced by waterflooding is moved through the reservoir to the producers by the pressure gradient created between the injector and the producer. Simultaneous production and injection could lead to variable regions of stress response in the grid with regions around the producer experiencing pressure energy loss resulting in compression of the sand grains while region close to the injector experiencing increase in pressure which could potentially cause volumetric dilation.

The methodology for coupling stress dependent relative permeability functions and numerical simulation discussed in the previous chapter is investigated using two water injection examples. However, a depletion case was also carried out to study the effect of compression alone on the production profile.

Detailed static and dynamic data and the procedure for the construction of the reservoir and geomechanical grids are presented in the following sections. In addition, the initialization of the models and production forecast for the uncoupled and coupled cases are described.

4.2 Water Injection Scheme

4.2.1 Description

Ideally, a fully validated Society of Petroleum Engineers' (SPE) case would have been adopted for this study but unfortunately, no example currently exists for the case of geomechanically influenced relative permeability functions. Consequently, the general characteristics of the model used in Problem 4 in Dean et al. (2003) were employed in this work. It was chosen because of its simplicity and availability of basic data needed to perform reservoir-geomechanical simulation. Nevertheless, some adjustments were made to some of the original data to suite the scope of this study and because of the modifications made to the original data, no attempt was made to reproduce the results from Dean et al., (2006).

4.2.2 Simulation Model and MEM

4.2.2.1 Simulation Grid

The structural frame for both the reservoir and geomechanical models were built using JewelSuite^{TM}. The flow grid shown in Figure 4.1 contains 21 grid blocks in the x-direction, 21 grid blocks in the y-direction and 11 layers, for a

total of 4,851 grid blocks. The x-y dimensions for each grid block are 19 m by 19 m and each layer is 6.1 m thick. The depth to top of the grid is 1219.2 m. Constant initial in-situ porosity of 27% was used throughout the grid, whereas, variable horizontal permeabilities of 5, 100, 20, 20, 20, 100, 20, 20, 100, 20, 20 md (Figure 4.2) were applied in each of the layer, from the top to the bottom. The ratio of vertical to horizontal permeability is 0.01.

The initial reservoir pressure at 1222.2 m is 11,825 kPa, and the initial oil and water saturation are 80% and 20%. The bubble point pressure at initial condition is 3500 kPa, the oil compressibility is 4.35E-07 1/kPa and the rock compressibility is 4.47E-05 1/kPa at 11,825 kPa. The model is a typical case of a volumetric reservoir, as no gas-oil or oil-water contacts were defined.

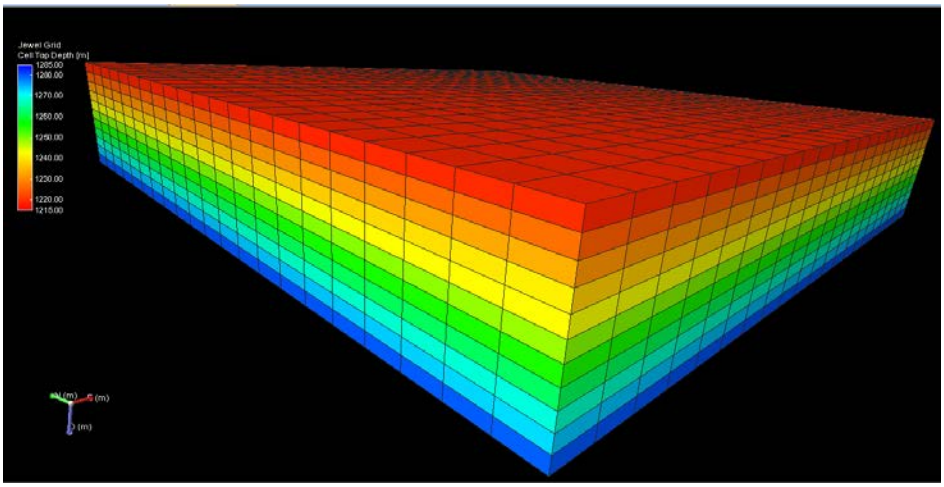

Figure 4.1: Flow grid

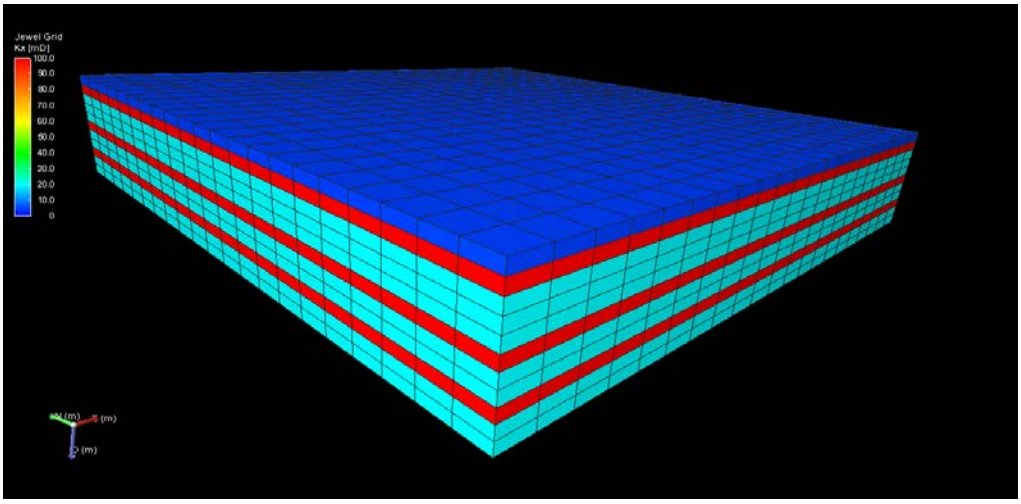

Figure 4.2: Vertical Variation in Horizontal Permeability. The scale varies between 0 to 100 mD

4.2.2.2 Mechanical Earth Model

The mechanical earth model (MEM) has the same dimension, grid size and layers as the reservoir model. The initial overburden stress at the top of the grid is 27,580 kPa and an overburden gradient of 22.6 kPa/m was applied throughout the model's vertical depth (Dean et al., 2003). Unlike Dean et al., maximum and minimum horizontal stress values were specified. Equation 4.1 was used in estimating the minimum horizontal stress using a fracture gradient constant (k) of 0.4 and the maximum horizontal stress was calculated using a horizontal to vertical stress ratio of 0.72. Normal hydrostatic fluid pressure gradient of 9.65 kPa/m was applied throughout the model. Young's modulus and Poisson's ratio values of 10.0 GPa and 0.3, respectively, were specified and were used in computing the bulk and shear moduli for the rock. Table 4.1 contains the full mechanical properties used in populating the MEM.

$$\sigma_{h\min} = k\sigma_v + (1-k)P_p \quad \text{.....4.1}$$

Properties	**Values**
Young's Modulus (GPa)	10.0
Poisson Ratio	0.30
Bulk Modulus (GPa)	8.33
Shear Modulus (GPa)	3.85
Density (g/cm3)	2.20
Overburden @ Top of Grid (kPa)	27580

Table 4.1: Elastic and Mechanical Properties

4.2.3 PVT Model

The PVT Table used for the initialization of the simulation model was generated inside CMG's Builder™ using the correlation shown in Table 3.0. The parameters in Table 4.2 were used as input to create the pressure-dependent oil and gas data (Table 4.3) used in the simulator. The matched PVT parameters for the oil bubble point pressure are shown in Appendix E. The density properties used were at surface condition of 101.32 kPa. The reservoir fluid used has a stock tank oil gravity of 28 ^{o}API and a gas gravity of 0.65. The water density is 990 kg/m^3, while the viscosity and compressibility are 1 cp and 4.57E-7 1/kPa respectively at a reference pressure of 101.33 kPa.

Properties	Values
Initial Reservoir Pressure (kPa)	11852
Bubble Point Pressure (kPa)	3500
Reservoir Temperature (oC)	60
Oil Formation volume factor	1.08
Oil Density (kg/m3)	886
Gas Gravity	0.65
Oil Viscosity	4.112

Table 4.2: PVT Input Data

P kPa	R_s m^3/m^3	B_o m^3/m^3	B_g m^3/m^3	Viso cP	Visg cP
101.325	0.557	1.036	1.148	6.650	0.012
554.482	1.792	1.038	0.208	6.251	0.012
781.060	2.481	1.040	0.147	6.048	0.012
1234.220	3.959	1.043	0.092	5.656	0.012
1687.370	5.539	1.046	0.067	5.289	0.012
2140.530	7.200	1.049	0.052	4.953	0.012
2593.690	8.929	1.053	0.043	4.645	0.013
3046.840	10.718	1.056	0.036	4.366	0.013
3500.000	12.559	1.060	0.031	4.113	0.013
9800.000	41.819	1.124	0.010	2.175	0.015
16100.000	75.424	1.203	0.006	1.448	0.018

Table 4.3: Pressure-Dependent Oil and Gas Data

4.2.4 Rock-Fluid Properties

The endpoint scaling option was used to generate the relative permeability

values shown in Table 4.4. The table end points values provided are: the relative permeability to water (k_{rw}) at residual oil saturation (S_{orw} = 0.30) of 0.391, relative permeability to oil (kro) at irreducible water saturation (S_{wir} = 0.20) of 0.510. Corey water saturation exponent of 4 was used, while 2 was used for the remaining saturation exponents. Other parameters and values are shown below in Table 4.4, and Figures 4.4 and 4.5. The different relative permeabilities plots represent no displacement condition.

Oil-water relative permeability is allowed to change as stress changes while the liquid-gad remains unchanged since no gas was produced. The solution gas was not allowed to come out of solution during production by keeping the minimum well bottom oil pressure above the bubble point pressure.

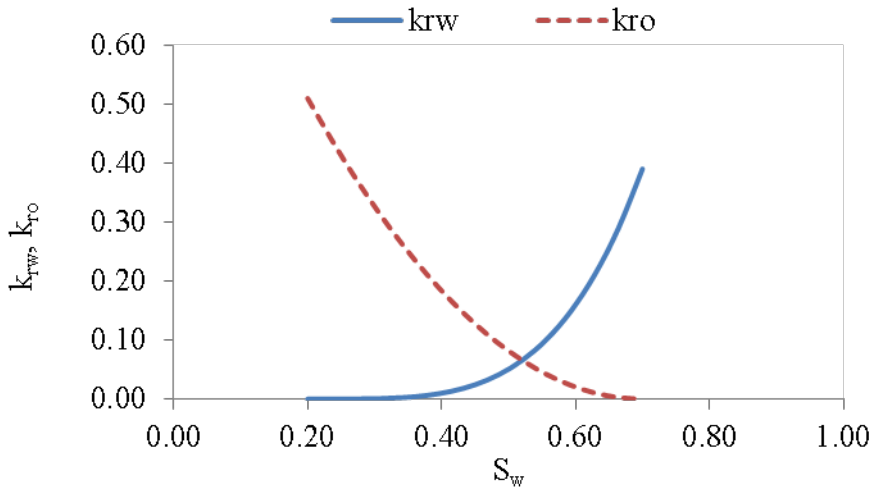

Figure 4.3: Water-oil relative permeability – initial conditions.

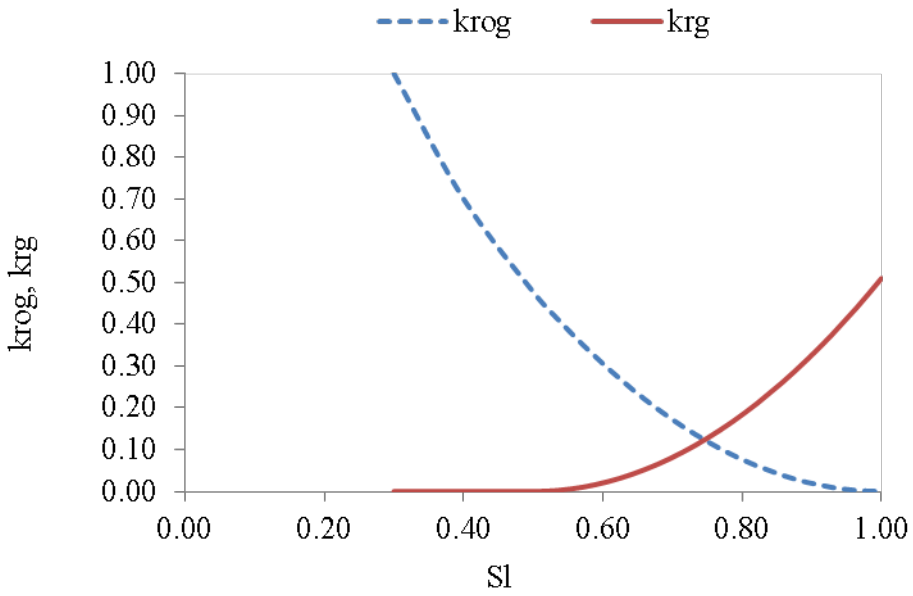

Figure 4.4: Liquid-gas relative permeability – initial conditions.

Sw	Krw	Krow	Sl	Krg	Krog
0.200	0.0E+0	0.510	0.500	0.477	0.000
0.236	1.0E-5	0.440	0.536	0.411	0.003
0.271	1.6E-4	0.375	0.571	0.351	0.010
0.307	8.2E-4	0.315	0.607	0.295	0.023
0.343	0.003	0.260	0.643	0.243	0.042
0.379	0.006	0.211	0.679	0.197	0.065
0.450	0.024	0.128	0.750	0.119	0.128
0.521	0.067	0.065	0.821	0.061	0.211
0.557	0.102	0.042	0.857	0.039	0.260
0.629	0.211	0.010	0.929	0.010	0.375
0.664	0.290	0.003	0.964	0.002	0.440
0.700	0.391	0.000	1.000	0.000	0.510

Table 4.4: Two-Phase Relative Permeability Table

4.2.5 Model Initialization

Similar to Dean et al., (2003) the model contains a quarter of a five-spot injection pattern with the oil production and water injection wells located in opposite corners of the grid, and both having completions in all the 11 layers.

Each of the wells has a radius of 0.11 m and a geometric factor of 0.29. Since the well was located at the edge of the grid boundary; a quarter of its normal drainage radius was therefore used in the simulator. Figure 4.5 shows the location of the wells.

The model was initialized to be undersaturated using one equilibrium region based on one fluid property indicated, with relative permeability region defined for each of the grid blocks. At time zero the saturation and pressure distribution in the model show no-flow situation, indicating that the model was at hydrostatic equilibrium. The initialization results are discussed in Chapter 5

The model was populated with the stress values discussed above, 3D view of the initial vertical stress values are shown in Figure 4.6, while Figure 4.7 shows the corresponding strain values which are all zero after initialization following the boundary and initial displacement prescribed at the top, sides and bottom of the geomechanical grid. The lateral displacement and the vertical displacement at the bottom of the model are all zero, while the top surface of the model is free to move vertically as shown in Figure 4.8.

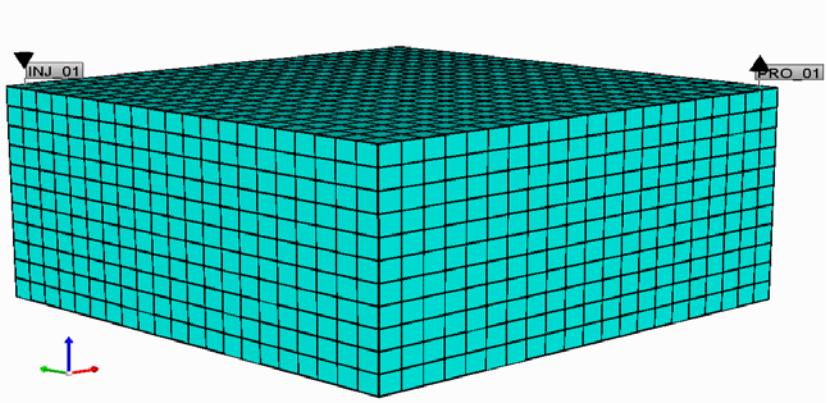

Figure 4.5: Location of the production well and injection well

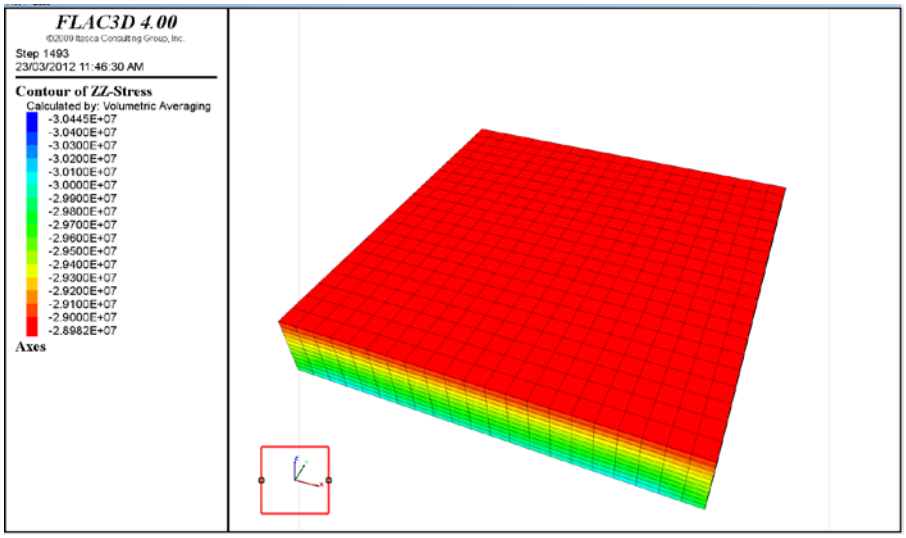

Figure 4.6: Initial Stress Condition in the ZZ-Direction

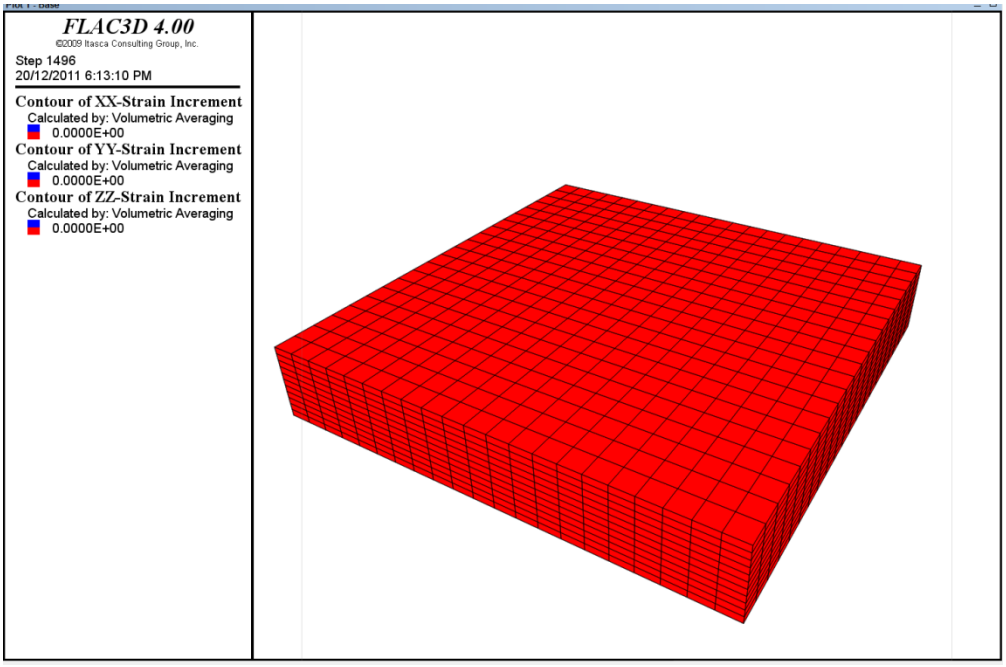

Figure 4.7: Strain values at equilibrium state – all values are zero

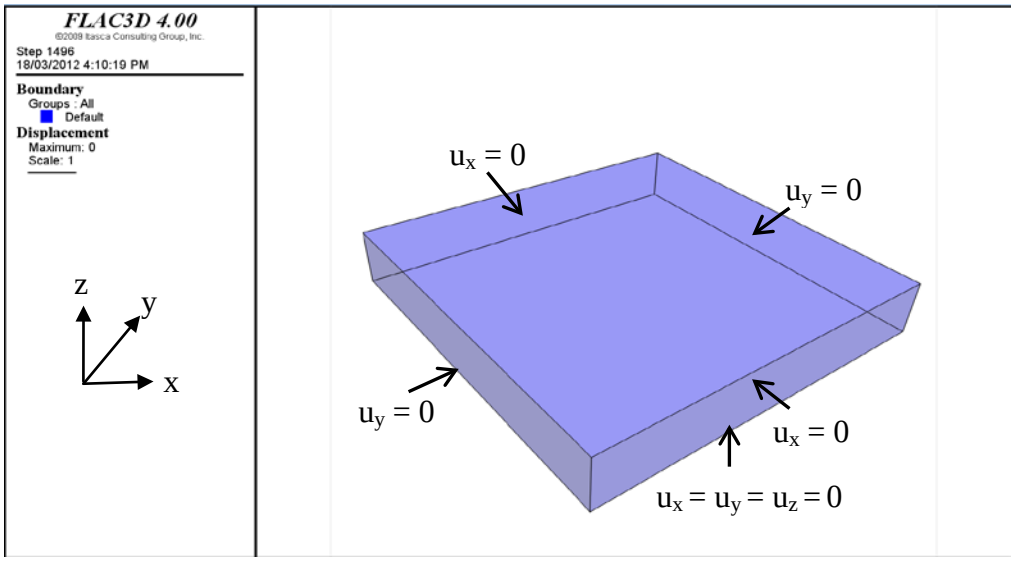

Figure 4.8: Boundary and Initial Conditions

4.2.6 Production Forecast and Sensitivities

Production forecasts were carried out for 30 years, with a time-step size of six months. The main objective of the production forecast was to generate and compare the production profile for the uncoupled and coupled cases. Two coupled simulation cases were carried out; using porosity and permeability as the coupling parameter (coupled_1) and using porosity, permeability and relative permeability as coupling parameters (coupled_2). The following set of producing rules were applied:

- Minimum bottomhole pressure - 4000 kPa
- Maximum injection pressure - 13019 kPa and 16738 kPa
- Maximum GOR - 500 m^3/m^3
- Maximum water cut - 95 %

- Minimum oil rate - 5 m^3/day

Two sensitivities runs were carried out and they are as follows: (1) initially depleting the reservoir to 9167 kPa at 730 days and injecting water at a pressure up to 13019 kPa and (2) depleting the reservoir pressure to 9167 kPa in 730 days and injecting water at a pressure up to 1673 kPa.

The waterflood simulations were carried out using maximum injection pressure and minimum bottom-hole pressure at the producer with the voidage replacement controlled by these pressures.

Chapter 5

Results and Discussion

The planned workflow for achieving coupling of stress induced changes in relative permeability with numerical simulation had been tested successfully. Details of the results of the simulation studies are presented in the following sections. Using the methodology described in Chapter 3 and data described in Chapter 4, stress induced porosity, permeability and relative permeability changes were evaluated for depletion and waterflood cases using the sequentially coupled approach. The primary focus was the effect of changes in initial in-situ stress on pore geometry and connectivity and the reservoir flow properties.

5.1 Depletion Case

5.1.1 Production Profile

Figure 5.1 illustrates the production profiles for the uncoupled simulation. The initial oil in place calculated for the model during initialization was 2300 Mm^3 and after running prediction for 15 years, about 82.20 Mm^3 of oil was produced, representing 3.57% of oil recovery.

Oil production rate declined rapidly and continuously from initial value of 82.92 m^3/day to about 15.41 m^3/day in 2008 days until the well hit the specified minimum oil rate of 5 m^3/day in 3468 days thereby 'shutting-in' due to the violation of the production constraint. It would be observed that the GOR remained constant throughout the production interval. Equally there was no water

production with the oil during the entire production interval, meaning there is the absence of water drive.

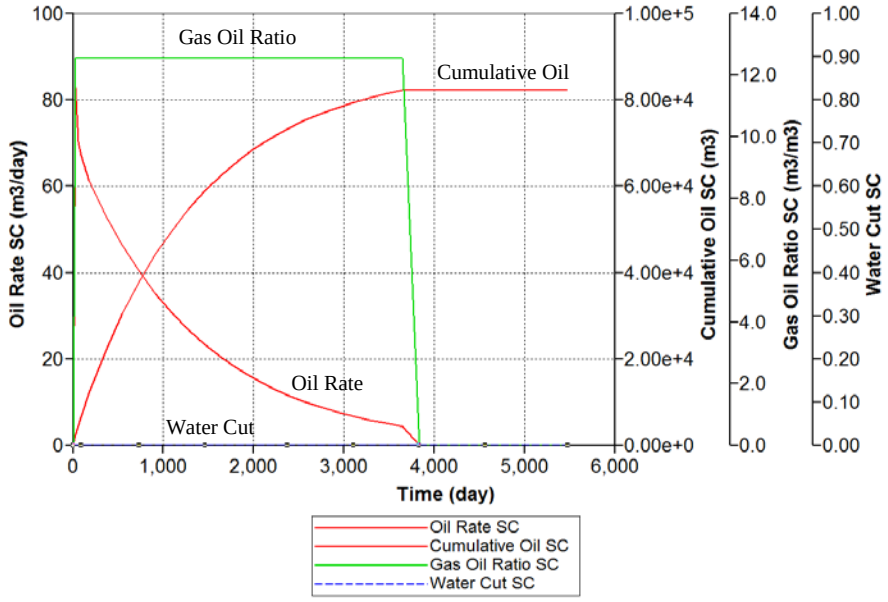

Figure 5.1: Production profile - uncoupled simulation

A total of 82.20 Mm^3 (3.57% recovery) of oil was produced from the uncoupled model. As shown in Figure 5.2 and Table 5.1, the inclusion of the compression effects caused the total oil predicted by the coupled_1 model to drop from 82.20 Mm^3 to 80.65 Mm^3 (3.51%). There was a further drop in the oil production to 78.86 Mm^3 (3.47%) as predicted by the coupled_2 model when stress dependent relative permeability is included in the coupled simulation.

The only source of energy driving oil towards the wellbore is compaction, since there was no other form of natural support present. As the reduction in pore volume occurs with decline in pressure, oil close to the production well is forced out of the pore space to the wellbore. The reservoir under this drive mechanism is

characterized by a constant gas-oil ratio that is equal to the gas solubility at the bubble point pressure. This driving mechanism is considered the least efficient driving force and usually results in the recovery of only a small percentage of the total oil in place (Tarek et al., 2001).

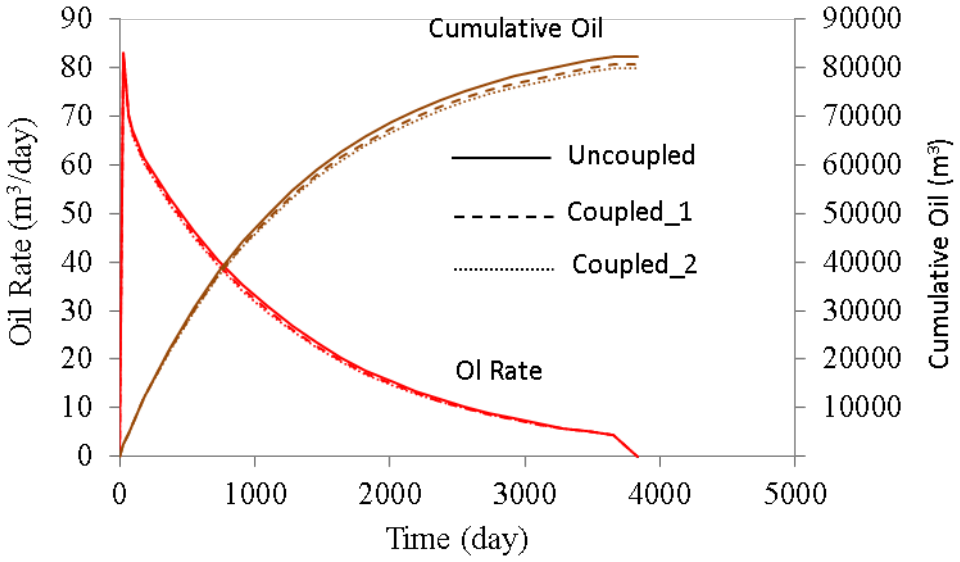

Figure 5.2: Production profile– uncoupled, coupled_ 1 and coupled_ 2

Sub-cases	**OOIP (Mm^3)**	**Cumulative Production (Mm^3)**	**Oil Recovery (%)**
Uncoupled	2300	82.20	3. 57
Coupled_1	2300	80.65	3.51
Coupled_2	2300	79.86	3.47

Table 5.1: Summary of cumulative production and recovery factor

5.1.2 Pressure Response

The average reservoir pressure declined continuously from its initial value of 11825 kPa to 4813 kPa in 3468 days, about 59.30% decline (Figure 5.2). The rapid decline in reservoir pressure can be attributed to the fact that no adjoining aquifer or gas caps are available to provide a replacement for the oil withdrawal. Also, gas was not liberated from the oil for expansion drive as the bubble point pressure was never attained, and because liquids and rocks are only slightly compressible.

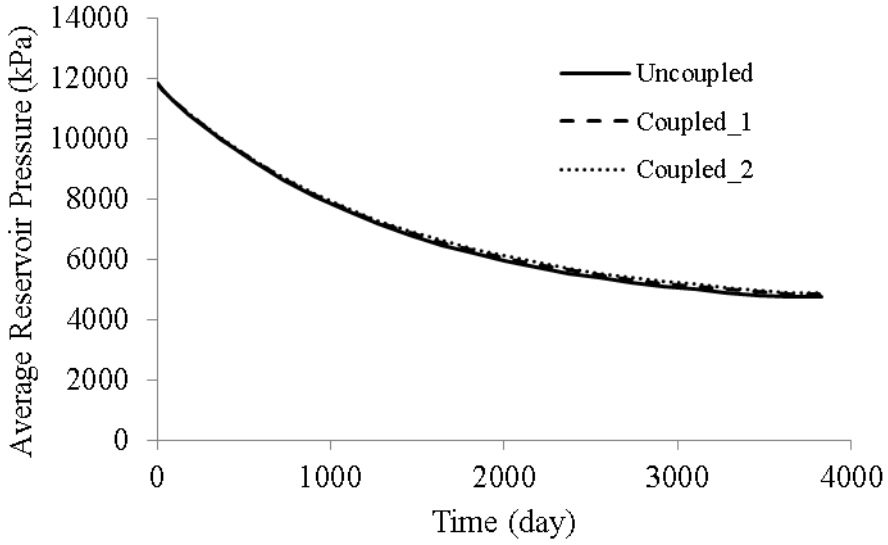

Figure 5.3: Reservoir Pressure - uncoupled and coupled simulation

The slight difference in the pressure responses between the uncoupled and coupled simulations in Figure 5.3 is ultimately due to the small difference in the production rate. The rate of fluid withdrawal is proportional to the decline in reservoir pressure; therefore the uncoupled model experienced the highest decline

in pressure followed by the coupled_1. The slight increase in pressure over the coupled_1 model by the coupled_2 model is due to the inclusion of stress dependent relative permeability in the coupled simulation.

5.1.3 Geomechanical Responses

As production lowers the pore pressure, additional stress is transferred to the rock structure during production, resulting in adjustment in total and effective stress. Horizontal and vertical stresses increase due to the reduction in the reservoir pore pressure (increased loading). As shown in Table 5.2, there was an increase in the vertical stress for grid block number 642 (block address 12 10 2) from 27.80 MPa to 30.20 MP at the end of simulation (5475 days). The change in the stress field results in compression of the grid and pore volume decreasing by 2.18% (Figure 5.4). Grid blocks closer to the production well experienced more reduction in bulk volume compared to the grid block in the far field.

			Time	0	0	0	5475	5475	5475
GB	I	j	k	sxx (Pa)	syy (Pa)	szz (Pa)	sxx (Pa)	syy (Pa)	Szz (Pa)
1	1	1	1	-2.0E+07	-1.8E+07	-2.8E+07	-2.0E+07	-1.9E+07	-2.9E+07
2	2	1	1	-2.0E+07	-1.8E+07	-2.8E+07	-2.1E+07	-1.9E+07	-3.0E+07
3	3	1	1	-2.0E+07	-1.8E+07	-2.8E+07	-2.1E+07	-1.9E+07	-3.0E+07
4	4	1	1	-2.0E+07	-1.8E+07	-2.8E+07	-2.1E+07	-1.9E+07	-3.0E+07
642	12	10	2	-2.0E+07	-1.8E+07	-2.8E+07	-2.1E+07	-1.9E+07	-3.0E+07
643	13	10	2	-2.0E+07	-1.8E+07	-2.8E+07	-2.1E+07	-1.9E+07	-3.0E+07
644	14	10	2	-2.0E+07	-1.8E+07	-2.8E+07	-2.1E+07	-1.9E+07	-3.0E+07
4811	2	20	11	-2.1E+07	-1.9E+07	-2.9E+07	-2.1E+07	-1.9E+07	-2.9E+07
4812	3	20	11	-2.1E+07	-1.9E+07	-2.9E+07	-2.1E+07	-1.9E+07	-2.9E+07
4813	4	20	11	-2.1E+07	-1.9E+07	-2.9E+07	-2.1E+07	-1.9E+07	-2.9E+07

Table 5.2: Change in in-situ stress

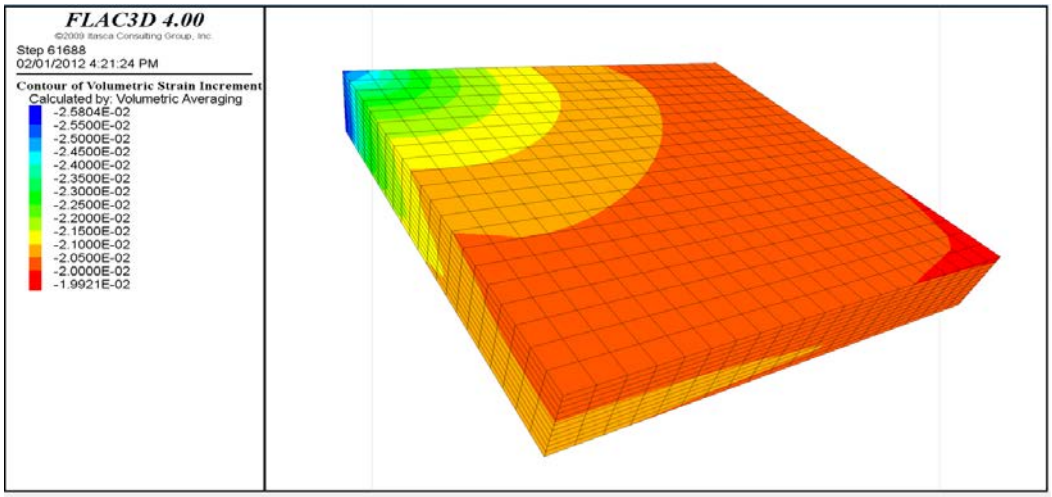

Figure 5.4: Volumtric strain response at the end of simulation

5.1.4 Porosity and Permeability Responses

Figures 5.5, 5.6, 5.7 and 5.8 illustrate changes in porosity and permeability values at initial condition and at the end of simulation. Porosity and permeability decreased in response to the increase in mean effective stress due to the decline in reservoir pressure. As clearly shown in Tables 5.3 and 5.4, grid block number 618 (block address: 9 9 2) experienced reduction in porosity from 0.27 to 0.25 and permeability from 100 md to 80.50 md in the second layer.

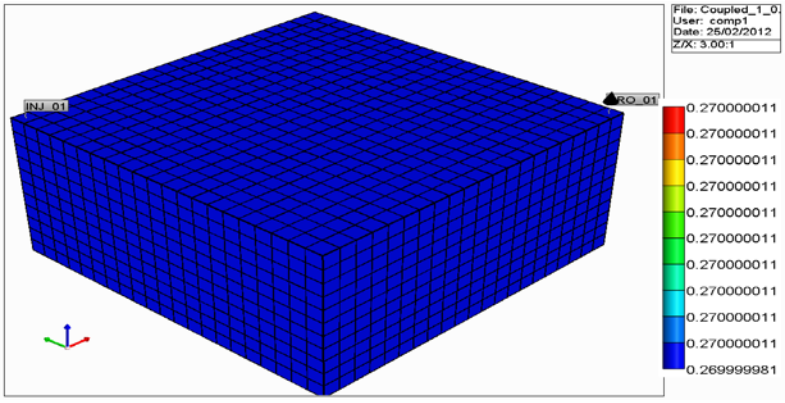

Figure 5.5: Porosity at Initial Condition**.**

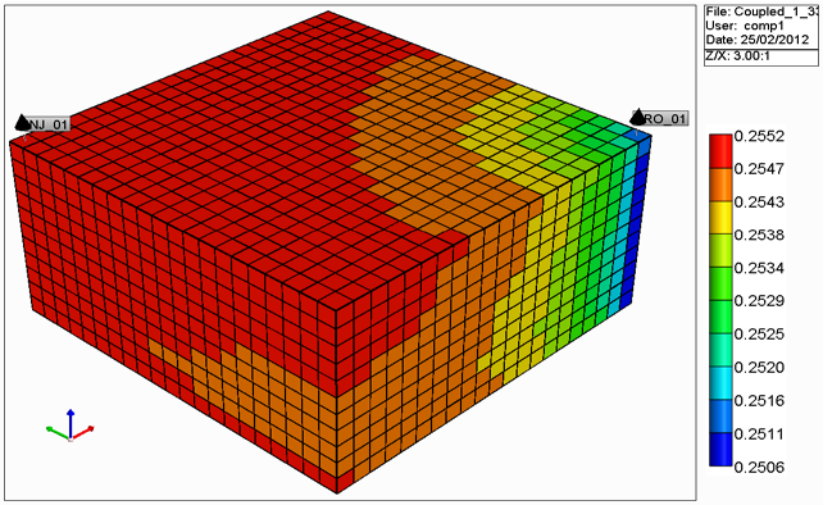

Figure 5.6: Porosity Response at the End of Simulation

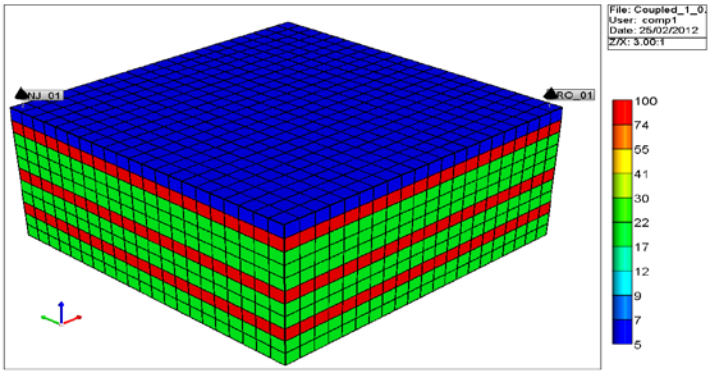

Figure 5.7: Permeability at Initial Condition

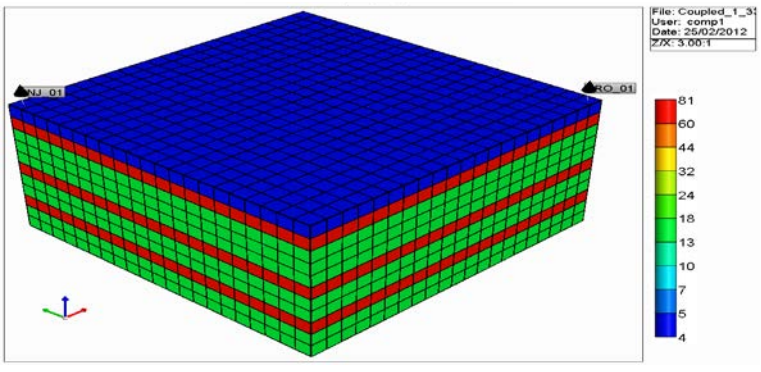

Figure 5.8: Permeability Response at the End of Simulation

GB	i	j	Time Step	Original	Original	Original	Current	Current	Current
				0	0	0	33	33	33
			k	Perm ii (mD)	Perm jj (mD)	Perm kk (mD)	Perm ii (mD)	Perm jj (mD)	Perm kk (mD)
1	1	1	1	5	5	0.05	4.043	4.043	0.040
2	2	1	1	5	5	0.05	4.038	4.038	0.040
3	3	1	1	5	5	0.05	4.038	4.038	0.040
618	9	9	2	100	100	1	80.500	80.500	0.805
619	10	9	2	100	100	1	80.448	80.448	0.804
620	11	9	2	100	100	1	80.392	80.392	0.804
3321	3	12	8	20	20	0.2	16.117	16.117	0.161
3322	4	12	8	20	20	0.2	16.114	16.114	0.161
3323	5	12	8	20	20	0.2	16.111	16.111	0.161

Table 5.3: Permeability Response

				Original	Current
Time Step				0	33
Variable	i	J	k	Porosity	Porosity
Block/Zone #					
1	1	1	1	0.270	0.255
2	2	1	1	0.270	0.255
3	3	1	1	0.270	0.255
618	9	9	2	0.270	0.255
619	10	9	2	0.270	0.255
620	11	9	2	0.270	0.255
3321	3	12	8	0.270	0.255
3322	4	12	8	0.270	0.255
3323	5	12	8	0.270	0.255

Table 5.4: Porosity Response

5.1.5 Shift in Relative Permeability

The endpoint relative permeability values exhibit a direct relationship with porosity for this model while the endpoint saturation values show an inverse relationship with porosity. The shift in the relative permeability values with

changes in stress within the well drainage area is illustrated using grid block number 20 (block address 20 1 1) shown in Figure 5.8.

Volumetric compression of the grid particularly in the well drainage area caused reduction in the initial in-situ k_{ro} from 0.510 to 0.429 and the final in-situ k_{rw} from 0.391 to 0.277 as well as an increase in the S_{or} from 0.30 to 0.37 and irreducible water from 0.20 to 0.29. The upper part of the k_{ro} curve shift to the right, up to k_{ro} value of 0.14 towards the tail end after which it shift to the left as S_w further increases. Similarly, the tail end of the k_{rw} curve up to S_w value of 0.53 shift to the right, while to the left as S_w further increase. Both the residual oil saturation and the irreducible water saturation increased.

To the left of Table 5.5 is the relative permeability table at the start of simulation and to the right is the relative permeability table at the end of simulation. In the Table, the value of the porosity multiplier (Poro*) is shown to decrease from 1.000 to 0.934.

As mentioned in Section 3.72, the geomechanical shift in the relative permeability is synonymous with the effect of wettability change on relative permeability. In this case, the neutral point shifting in the direction of decrease in relative permeability and saturation, that is tending towards oil wet (Figure 5.8). The shift in the relative permeability curves and the neutral point is not necessarily due to change in wettability as described by Abdulrahman and Khairy (2005) since the rock mineralogical composition is not altered by geomechanics.

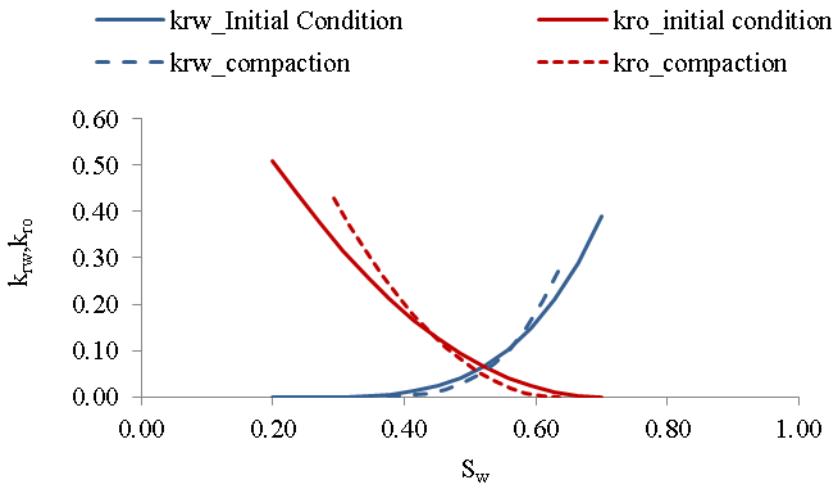

Figure 5.8: Shift in the Relative Permeability

		Original	Step	0		Current	Step	33
		Sw	Krw	Krow		Sw	Krw	Krow
Region ID	20	0.200	0.000	0.510	20	0.292	0.000	0.429
Model Type	2	0.236	0.000	0.440	2	0.316	0.000	0.370
Avg Vol Strain	0.000	0.271	0.000	0.375	-0.025	0.341	0.000	0.315
Poro*	1.000	0.307	0.001	0.315	0.934	0.365	0.001	0.265
Kro	0.510	0.343	0.003	0.260	0.429	0.390	0.002	0.219
Sor	0.300	0.379	0.006	0.211	0.365	0.414	0.005	0.177
Krw	0.391	0.414	0.013	0.167	0.277	0.439	0.009	0.140
Swi	0.200	0.450	0.024	0.128	0.292	0.463	0.017	0.107
Sgcon	0.000	0.486	0.042	0.094	0.000	0.488	0.030	0.079
Krg	0.477	0.521	0.067	0.065	0.477	0.512	0.047	0.055
Krog	0.510	0.557	0.102	0.042	0.510	0.537	0.072	0.035
Nw	4.000	0.593	0.149	0.023	4.000	0.561	0.106	0.020
No	2.000	0.629	0.211	0.010	2.000	0.586	0.150	0.009
Nog	2.000	0.664	0.290	0.003	2.000	0.610	0.206	0.002
Ng	2.000	0.700	0.391	0.000	2.000	0.635	0.277	0.000

Table 5.5: Change in Relative Permeability Table at the End of Simulation

5.2 Water Injection Case

5.2.1 Production Profile

5.2.1.1 Uncoupled Simulation

The production profiles for the uncoupled simulation for the two sensitivities cases (low and high injection pressure) are presented in Figures 5.9 and 5.10. For the low injection pressure case, oil production declined sharply from 83 m^3/day to 44 m^3/day at 730 days before the injection of water. However, oil production rate increased gradually to about 59 m^3/day in 6023 days due to gradual pressure buildups following the injection of water until the rate started dropping, due to encroachment of water and eventual water breakthrough in 6388 days. Water production increased steadily until the end of prediction (Figure 5.9). The cumulative oil production at the end of prediction (30 years) was 482 Mm3, representing 20.96% of oil recovery.

For the high injection pressure case, oil production declined sharply from 83 m^3/day to 44 m^3/day in 730 days, which was identical to the response seen for the low pressure injection case, and increased gradually to about 84 m^3/day in 4198 days due to the injection of water until the rate started dropping as a result of the eventual water breakthrough in 4389 days. The water cut increased steadily to 77% until the end of simulation (Figure 5.10). The cumulative oil production stood at 555 Mm^3, representing 24.1% of oil recovery and a 15% increase over the low injection pressure scenario.

The total production was a function of the individual contributions from each layer, permeability being the variable parameter. The initial water

breakthrough experienced in the model occurred in layers 2, 6 and 10 due to the high permeability. Production and injector volume in the model were mostly contributed by these layers with less contributions from other layers with low permeability (5 and 20 md). As shown in Figure 5.11 at 6205 days water breakthrough occurred in layer 2, while the water front was still far from the production well in layer 3. High permeability and high injection pressure improved the displacement process.

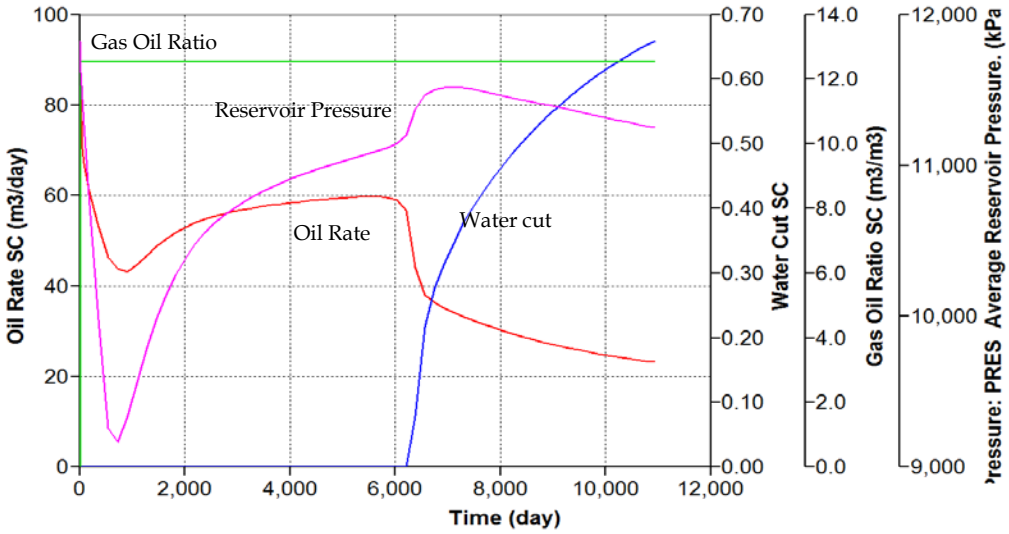

Figure 5.9: Production Rate – 13019 kPa Max. Injection Pressure.

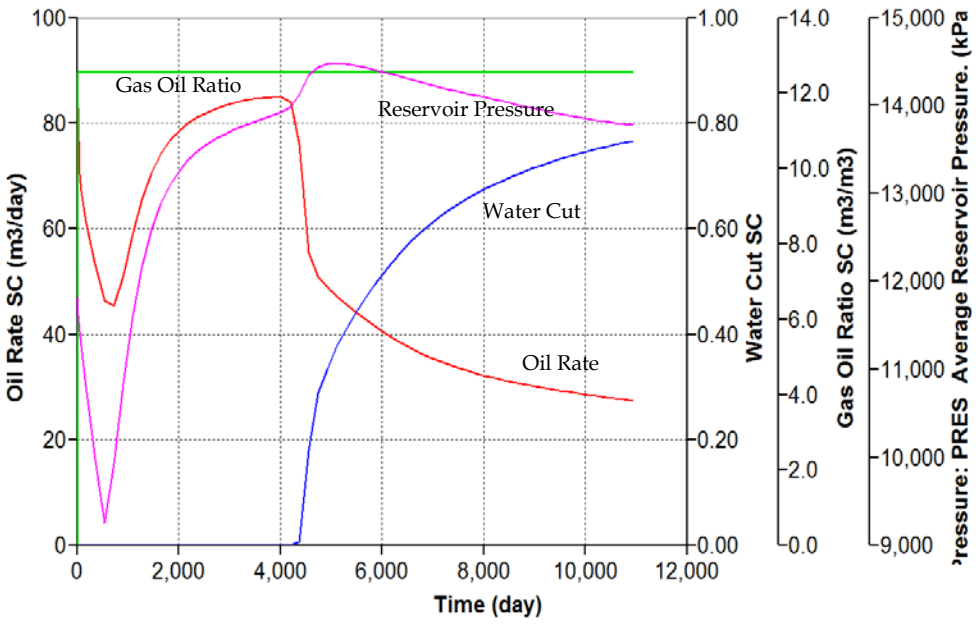

Figure 5.10:Production Rate – 16380 kPa Max. Injection Pressure.

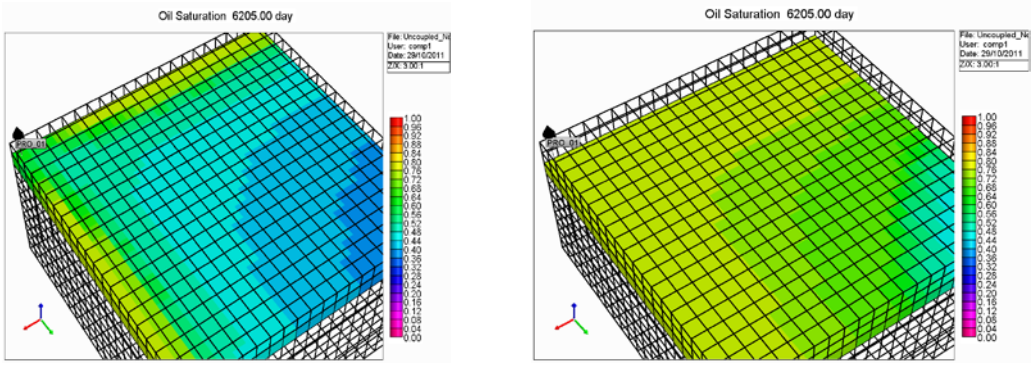

Figure 5.11: Water Front – Layer 2 and 3

5.2.1.2 Coupled Simulation

Inclusion of stress-induced changes in porosity and absolute permeability (Coupled_1) and relative permeability (Coupled_2), especially in the near wellbore region of the production well, the behavior of the reservoir-fluid pressure and an associated reduction in the productivity index revealed that these

models predicted lower cumulative oil production than the uncoupled simulation predictions, as shown in Figures 5.12, 5.13, 5.14 and 5.15.

As illustrated in Figure 5.12 with supporting values provided in Table 5.6, the inclusion of geomechanically influenced relatively permeability has clearly effected simulation predictions result in an 11% reduction in cumulative oil production in comparison to the uncoupled simulation – a decrease in oil production from 482 Mm^3 to 428 Mm^3. The coupled_1 simulations predicted a 7.5% reduction in cumulative oil production – a decrease in oil production from 482 Mm3 to 446 Mm3. Water breakthrough occurred in 7,118 days in the coupled_2 simulation, a significant delay in water production, compared to 6,388 days predicted by the uncoupled simulation and 6,753 days recorded for the coupled_1 simulation (Figure 5.12 and Table 5.7).

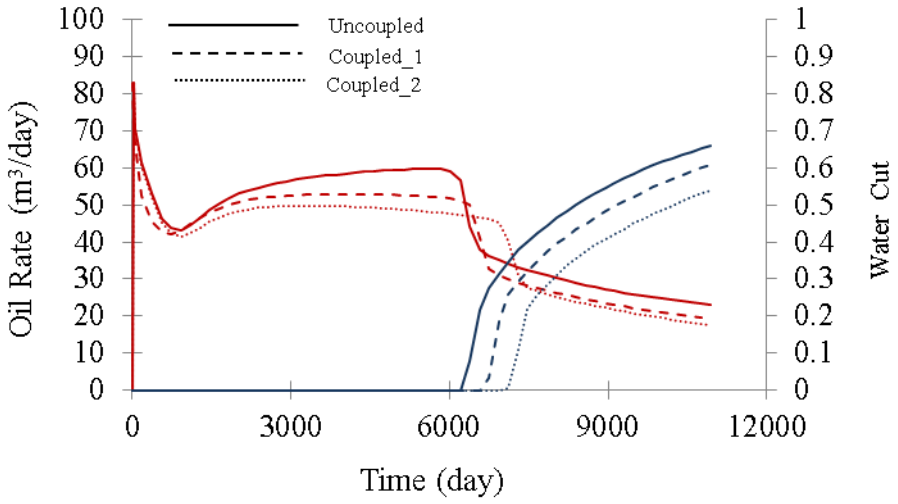

Figure 5.12: Production Rate - 13019 kPa Injection Pressure.

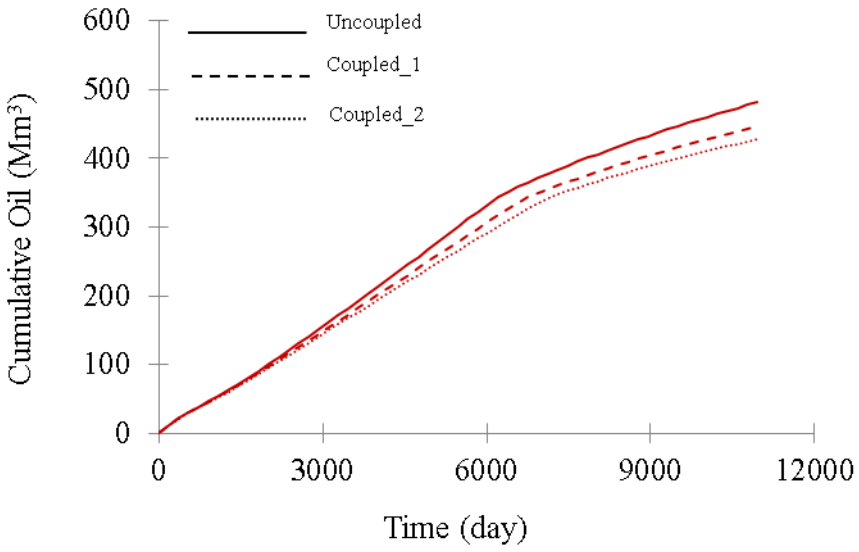

Figure 5.13: Cumulative production – 13019 kPa Injection Pressure

Increasing the maximum injection pressure from 13019 to 16738 kPa caused an increase in the cumulative oil production to 522 Mm^3 (Figure 5.14 and Table 5.6) as a result of the increase in the pressure gradient which caused more oil to be swept towards the producer. However, the production was still lower compared to the uncoupled and coupled_1 simulations because of the effect of the compaction-induced changes in porosity, permeability and relative permeability in the near wellbore region of the production well. Table 5.6 summarizes the recovery factor calculated for the different simulation cases. Very little water (0.22%) was produced in 4563 days in the coupled_2 simulation, the same time the water cut was 3.56% in the coupled_1 simulation. Significant water was actually produced after 4563 days in the coupled_2 simulation due to the loss in porosity, permeability and reduction in fluid movement close to the producer's near well bore area.

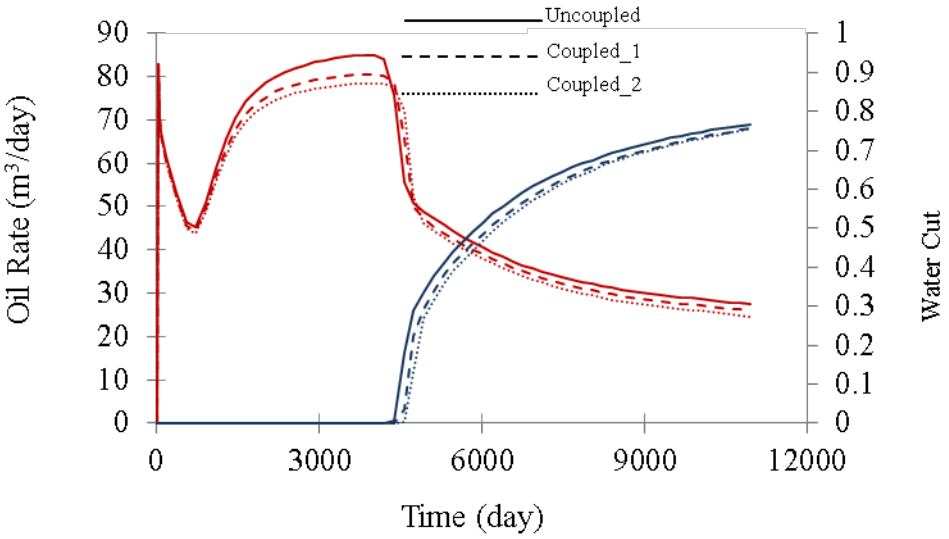

Figure 5.14: Production rate - 16738 kPa Injection Pressure

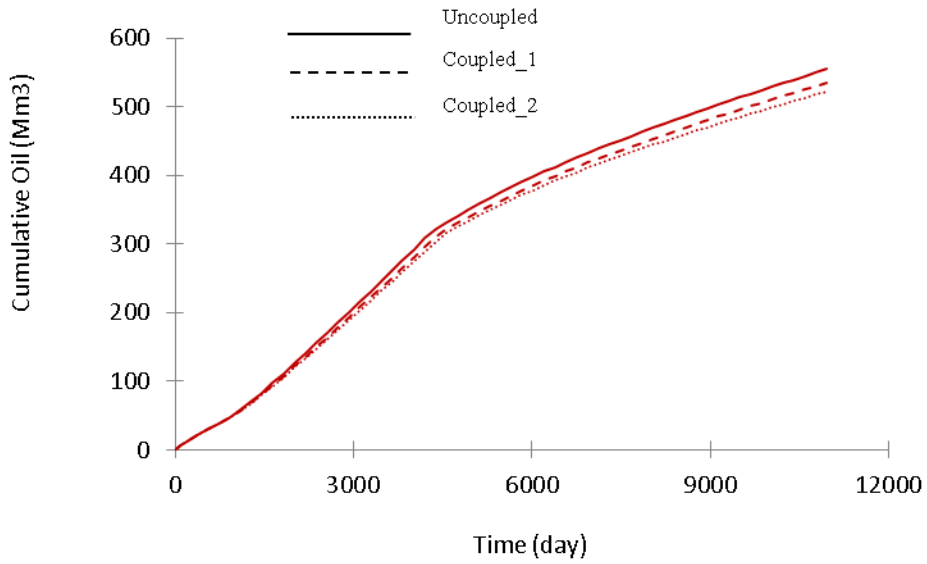

Figure 5.15: Cumulative Production – 16738 kPa Injection Pressure

Sub-cases (kPa)	Cum Oil (Mm^3) Uncoupled	Cum Oil (Mm^3) Coupled_1	Cum Oil (Mm^3) Coupled_2	Oil Recovery Uncoupled (%)	Oil Recovery Coupled_1 (%)	Oil Recovery Coupled_2 (%)
13019	482	446	428	20.96	19.39	18.61
16389	555	535	522	24.13	23.26	22.70

Table 5.6: Summary of Cumulative Oil Production and Recovery Factor

Sub-cases (kPa)	Breakthrough Time Uncoupled (day)	Breakthrough Time Coupled_1 (day)	Breakthrough Time Coupled_2 (day)
13019	6388	6753	7118
16389	4380	4563	4563

Table 5.7: Summary of Water Breakthrough Time

5.2.2 Pressure Response

For the low injection pressure case, the average reservoir pressure declined from 11825 kPa to 9167 kPa in 730 days, about 22.5% decline, before the injection of water (Figure 5.16). However, the pressure drawdown was controlled by the voidage replacement. This allowed the pressure to build-up again gradually and peaked at 11521 kPa in 7118 days, after which it declined slightly to 11250 kPa towards the end of the prediction due to water production.

For the high injection pressure case, the average reservoir pressure declined from 11825 kPa to 9256 kPa in 548 days, 21.7% decline (Figure 5.17). The pressure built gradually thereafter and peaked at 14272 kPa (above the initial reservoir pressure) in 6753 days after which it experienced a gradual decline down to about 13777 kPa at the end of the prediction run due to water production.

The pressure profile variations shown in Figures 5.16 and 5.17 for the

different simulation cases is related to the number of coupling parameters (porosity, permeability and relative permeability) included in the coupled simulation. As the effect of dilation propagates from the injector area towards the producer area after the initial pressure decline, there is an associated increase in porosity, permeability and volume of the displaced fluid. This results in an increase in the average reservoir pressure in most of the grid blocks except those that are near the production well.

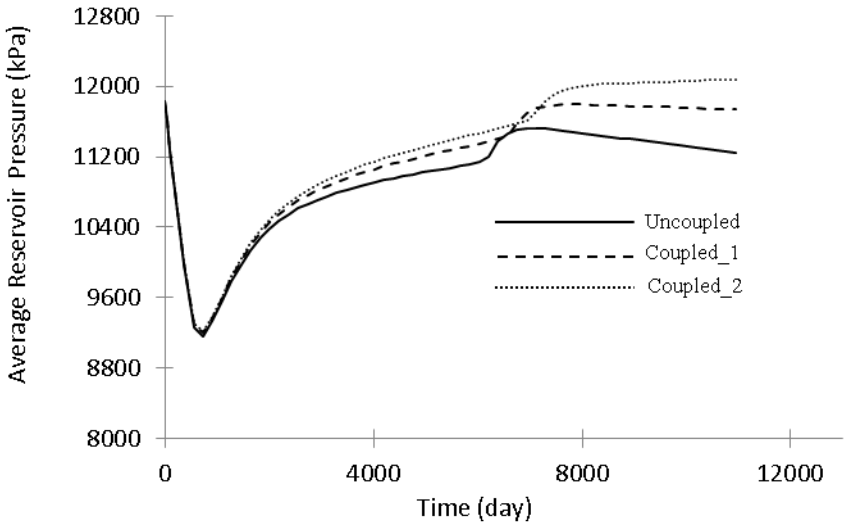

Figure 5.16: Pressure profile - injecting at 13019 kPa maximum.

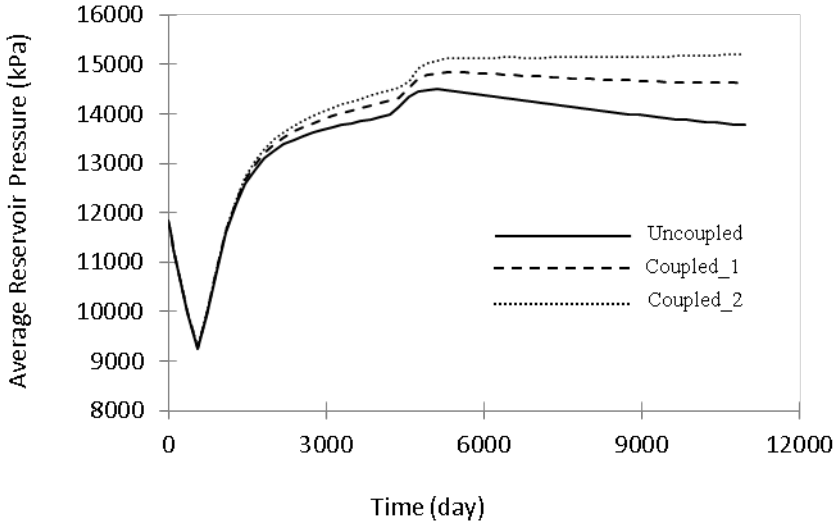

Figure 5.17: Production profile – injecting at 16738 kPa maximum.

Concurrently, the reduction in porosity, permeability as well as relative permeability especially in the production well's near wellbore region caused reduction in the inflow to the producer and subsequent liquid hold-up in the far area of wellbore. This reduced voidage compared to the uncoupled simulation helped minimize the decline in the average reservoir pressure. The net effect of the responses to the geomechanical processes in the entire grid resulted in increase in the average reservoir pressure for the coupled simulation compared to the uncoupled simulation.

5.2.3 Geomechanical Responses

Deformation from the disturbance of the reservoir by production/injection activities caused both compaction and dilation effects in different sections of the grid. The 3D view of the volumetric strain response from FLAC3D for the first

sensitivity case is shown in Figure 5.18. The decline in the reservoir pressure mostly around the production well caused a net increase in the mean effective stresses over time which caused a negative volumetric strain response as observed in FLAC3D and corresponding reduction in pore volume in some sections of the model.

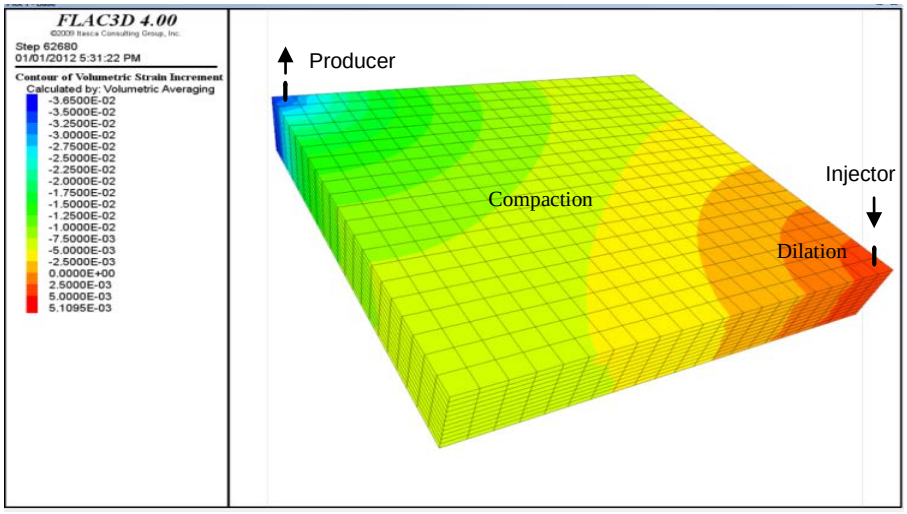

Figure 5.18: Volumetric Strain - injecting at 13019 kPa maximum.

This effect decreased towards the region around the injector, where the model experienced an increase in pore volume (positive volumetric strains). The injection pressure of 13019 kPa did not create a large pore pressure front that moved towards the production well. Volumetric compression is the dominant geomechanical process within the entire model aside from a few grid blocks in the region closer to the injector.

However, initially depleting the reservoir to 9166 kPa in 730 days and injecting up to 16389 kPa, instead of 13019kPa, allowed more areas even farther away from the injection well to experience a decrease in effective stresses and

corresponding increase in pore volume (positive volumetric response), as shown in Figure 5.19. The intensification of the dilation effect in the grid blocks even close to the production well is due to the increase in the pressure gradient between the injection and production well. The high pore pressure front moved toward the production well creating expansion in the grid blocks in the regions close to the production well. For this higher injection pressure case, dilatant or positive volumetric strains are the dominant geomechanical process controlling the grid response to the change in in-situ stress except in the near wellbore region of the production well.

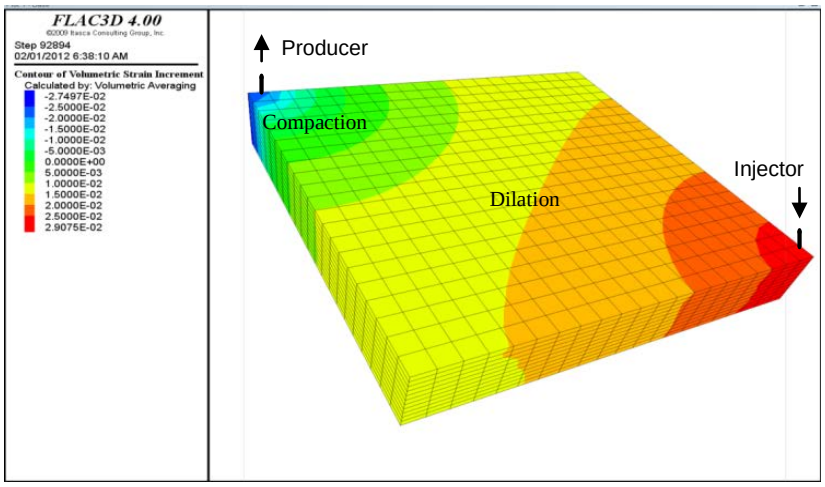

Figure 5.19: Volumetric Strain - injecting at 16738 kPa maximum.

5.2.4 Porosity and Permeability Responses

Porosity and permeability changed in response to the local stress regimes that induced compaction or dilation in each of the grid blocks in different sections of the model. Overall, grid blocks closer to the production well experienced net reduction in porosity and permeability, while grid blocks closer to the injector

experienced net increase in permeability and porosity after the commencement of injection up to the end of the simulation.

Few grid blocks in the region close to the injector experienced increase in porosity and permeability when the production forecast was carried out using 13019 kPa as the maximum injection pressure. However, an increase in porosity and permeability occurred in most of the grid blocks when 16738 kPa was used as the maximum injection pressure, except for few grid blocks in regions close to the production well due to the compaction effects resulting from fluid withdrawal, as illustrated in Figures 5.20, 5.21, 5.22 and 5.23. Porosity, initially at 0.27, increased 7.8% in the injector area, while it decreased gradually towards the producer area to about 0.25 or a 7.4% reduction. Meanwhile, permeability in the second layer increased from 100 to 131 md in the grid blocks close to the injector, but decreased gradually from 100 md to 85 md in grid blocks around the producer.

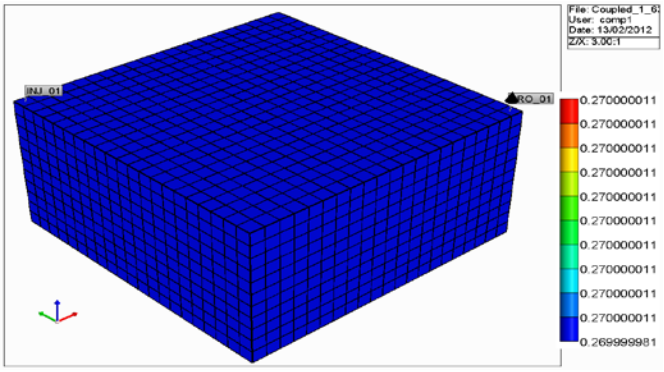

Figure 5.20: Initial Porosity

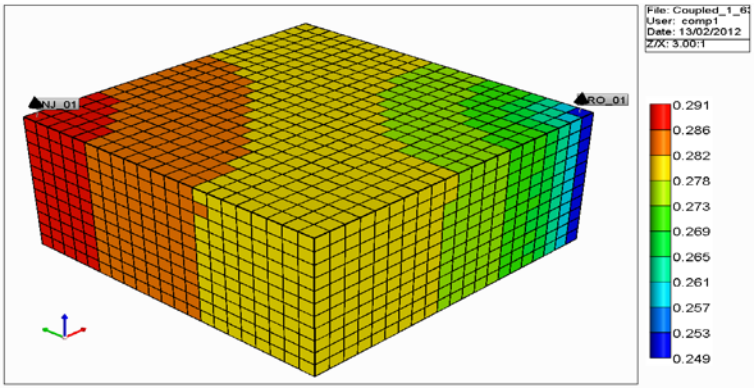

Figure 5.20: Porosity at end of simulation

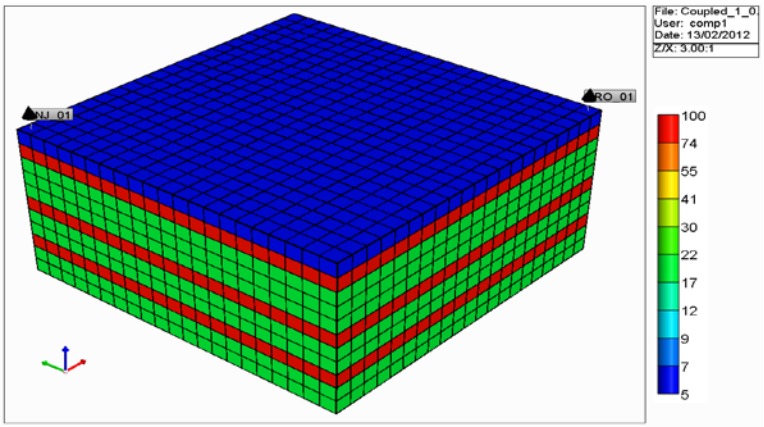

Figure 5.21: Initial permeability

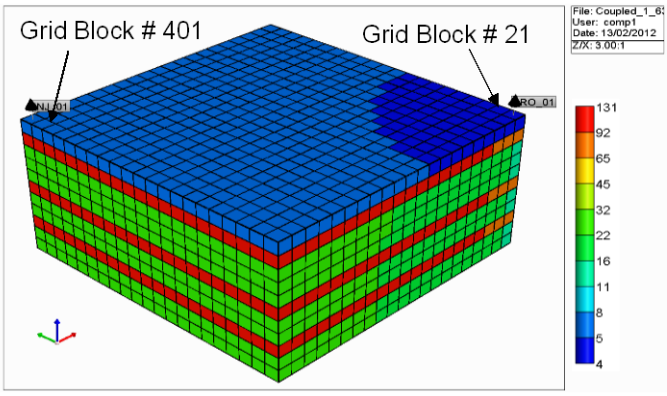

Figure 5.22: Permeability at end of simulation

5.2.5 Shift in Relative Permeability

The shift in the relative permeability values with changes in stress can be explained using the results from two grid blocks in the compaction and dilation regions in the second sensitivity case. Grid block number 21 (cell address 21 1 1), in the producer area as shown in Figure 5.23, experienced compaction (reduction in ϕ^*), and that caused the entire relative permeability to oil (k_{ro}) curve to shift to the left and the end point to decrease from 0.510 to 0.432 (Figure 5.24). Meanwhile, there was very little or no shift in the relative permeability to water (k_{rw}) curve up to water saturation value of 0.583, but a shift to the left as the water saturation further increased. The endpoint relative permeability to water $k_{rw}(S_{or})$ reduced from 0.391 to 0.281. There was also a reduction in the neutral point (points at which k_{rw} and k_{ro} are equal). The residual oil (S_{or}) increased from 0.30 to 0.36 thereby decreasing the mobile oil saturation slightly, while the irreducible water, S_{wir} increased from 0.20 to 0.24, decreasing the mobile water saturation by a small amount.

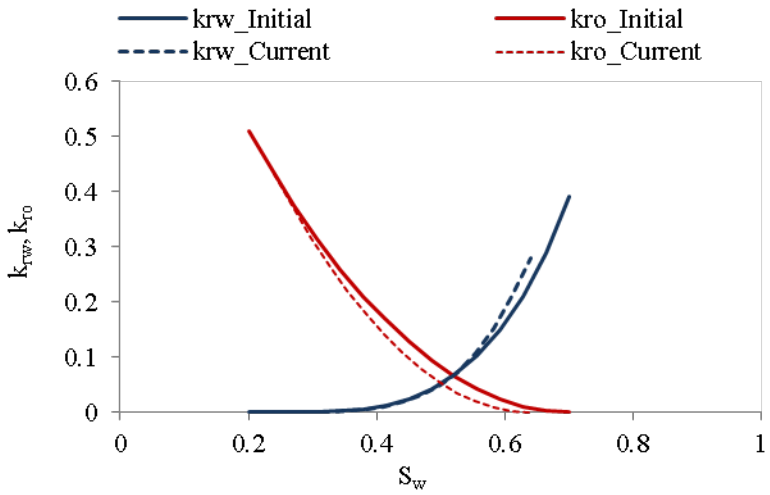

Figure 5.23: Shift in relative permeability for grid block number 21 (Compaction).

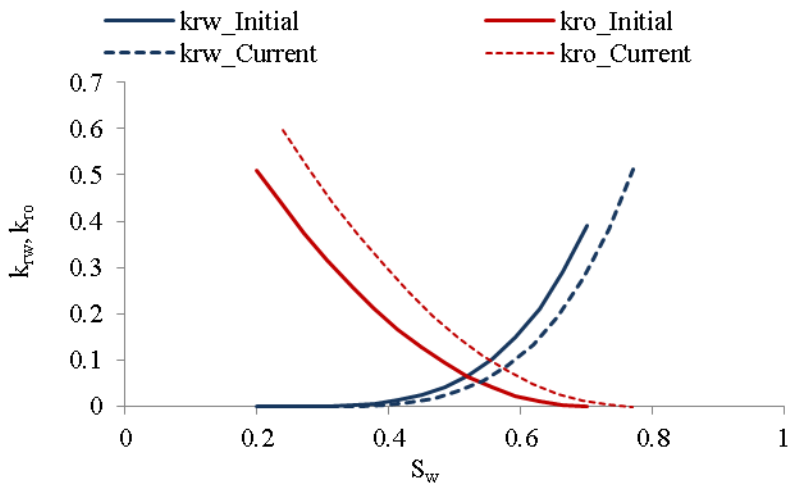

Figure 5.24: Shift in relative permeability for grid block 401 (Dilation)

Grid block number 401 (cell address: 2 20 1), shown in the injector near well bore region in Figure 5.23 experienced dilation and corresponding increase in ϕ^*. This creates a shift in the entire curve to the right and an increase in the end point k_{ro} from 0.510 to 0.597. The neutral point also increased, similar to the case of the effect of wettability on relative permeability in which the neutral point could be said to have shifted towards more water wet (Fig. 5.25). The S_{or} decreased from 0.30 to 0.23 thereby causing an increase in the mobile oil saturation, while the S_{wir} increased causing a corresponding reduction in the mobile water.

Increase in the pore size, pore throat size and possible reduction in capillary pressure experienced mostly around the injector and towards the production well made it easier for water to displace oil allowing more oil to be drained easily by water. However, the anticipated increase in oil production was lowered by the decrease in fluid flow due to reduction in porosity, permeability and relative permeability. The reduction in k_{ro} near the producer that also affected the

productivity index was never accounted for in either the uncoupled simulation or coupled_1 Simulation.

The fundamental issues with the shift in the relative permeability for individual grid blocks is the diverse value of endpoint mobility ratio compared to the single value both in the uncoupled simulation and coupled_1 simulation, in addition to spatial and temporal variation in the fractional flow and the whole effect on the displacement process.

The relative permeability curve endpoint values reduced in grid blocks that experienced compaction, while they increased in grid blocks dominated by the dilation process. Compaction caused reduction in the pore volume and increase in capillary pressure leading to an increase in immobile oil and water saturation. Dilation on the other hand caused a decrease in the residual oil saturation while the irreducible water saturation was initially increased as pore volume increased and later decreased at pore volume increased following the observation of Khan (2009) for the path of decreasing mean effective stress. The initial increase in irreducible water as pore volume increased can be attributed to increased pore sizes and porosity, causing more water to be required to line the pores (Khan, 2009) However, as the pore volume increased further, the capillary bound water saturation decreased.

5.2.3 Water Injection Volume

The waterflood performance for the two sensitivities cases (low and high injection pressures) is shown in Figures 5.26 and 5.27 for the different simulation cases. The oil recovery is higher for the uncoupled simulation likewise the volume

of water injected, while the recovery for the coupled_2 simulation was the lowest, also the volume of water injected. In the second sensitivity for example, about 881 Mm^3 of water was injected in the coupled_2 simulation case to produced 522 Mm^3 of oil at the end of simulation, which was 6.55% and 3.40% less than what was injected in the uncoupled and coupled_1 simulation (Table 5.8).

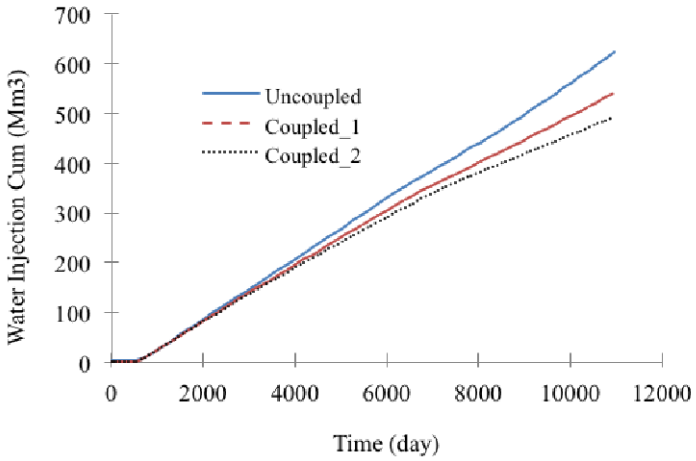

Figure 5.25: Cumulative water injection - injecting at 13019 kPa maximum.

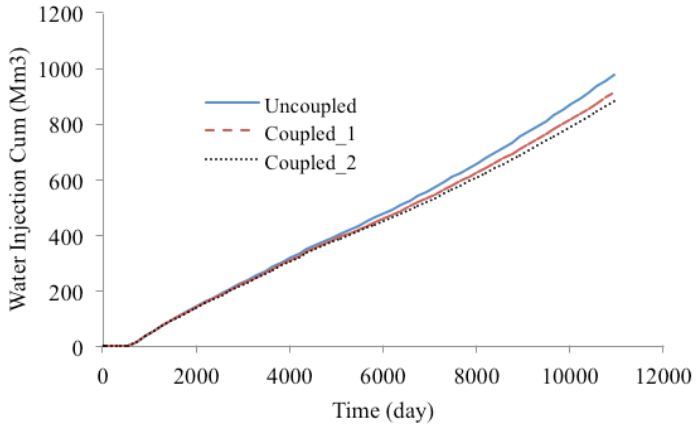

Figure 5.26: Cumulative water injection - injecting at 16738 kPa maximum.

Simulation Case	13019 kPa - Cum Water Injected (Mm3)	16738 kPa - Cum Water Injected (Mm3)
Uncoupled	621	977
Coupled_1	540	913
Coupled_2	491	882

Table 5.8: Cumulative Water Injected

5.2.4 Adjusting Only the Relative Permeability

Comparison of the performance when stress dependent relative permeability alone is used as the coupling parameter in the coupled simulation compared with all the other simulation cases is shown Figure 5.28 and 5.29. It can be observed that adjustment in the relative permeability alone has significant impact on recovery.

About 540 Mm^3 cumulative oil (Figure 5.29) was produced when relative permeability alone was used as the coupling term in the coupled simulation, 535 Mm^3 cumulative oil was obtained for porosity and permeability alone; and 522 Mm^3 when all the three parameters were used. Its total recovery was still lower compared to 555 Mm^3 obtained from the uncoupled simulation. The water breakthrough occurred the same time as in the case of the couple_1 simulation, with 8.25% water cut compared to 3.56% recorded for the coupled_1 simulation. When compared to the uncoupled simulation, the water breakthrough was delayed by 183 days.

The reduction in total production compared to the uncoupled simulation was

due mainly to stress dependent relative permeability effects in the near wellbore region due to the reduction in the inflow performance. Despite the increase in the relative permeabilities due to dilation in the other region, the decrease in the relative permeabilities due to compaction effects in the production well domain dominated the total production.

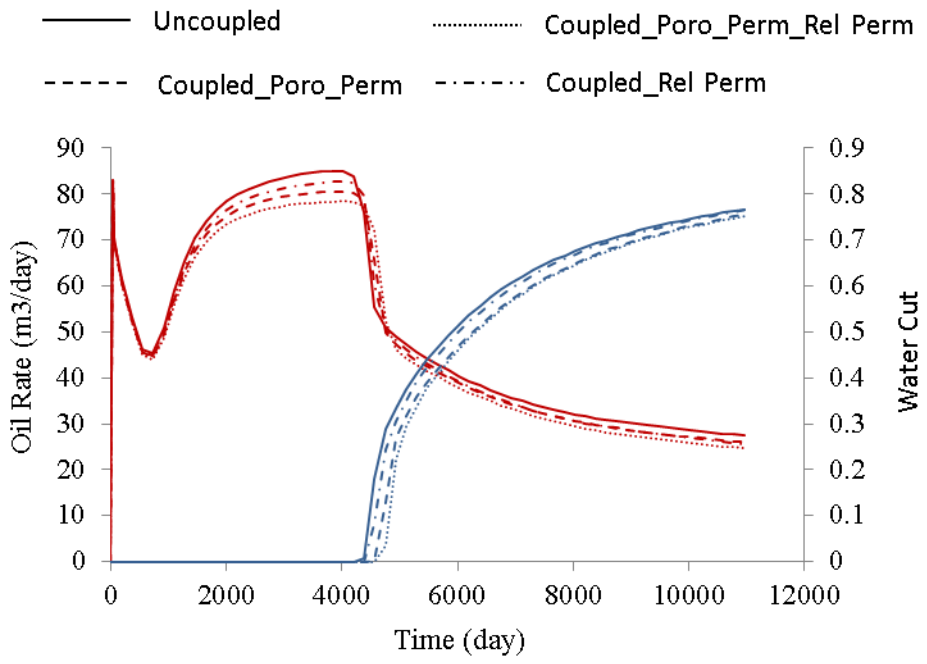

Figure 5.27: Production rate – adjustment to relative permeability alone

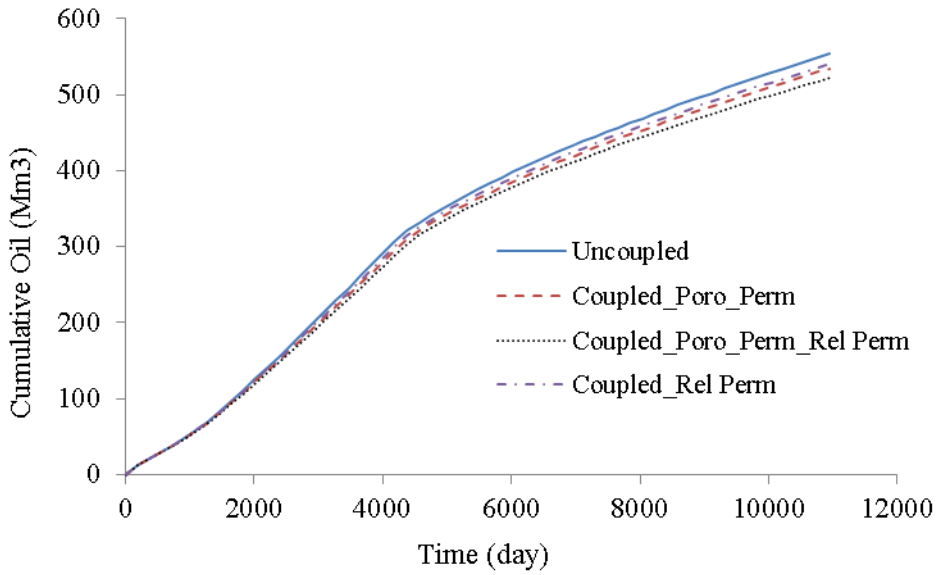

Figure 5.28: Cumulative production - adjustment to relative permeability alone.

Chapter 6

6.1 Conclusion

The procedure for coupling stress dependent relative permeability with numerical simulation was developed and tested successfully using the sequentially coupled reservoir geomechanical modeling approach. Neglecting the geomechanical impacts of production/injection activities could lead to possible error in production forecast especially for reservoirs under improved oil recovery scheme depending on the level of injection pressure and reservoir overburden. A more accurate production forecast could be obtained when the effects of geomechanics on porosity, permeability and relative permeabilities are properly accounted for. Relative permeability has a strong impact on grid saturation behavior which may not be modeled by coupled simulation with porosity and permeability as coupling term alone since they do not fully account for the mobile saturation. Stress dependent relative permeability has an effect on the reservoir inflow performance and therefore the well deliverability.

Adjustment to relative permeability end point values to match saturation profiles for stress sensitive reservoirs should include geomechanical processes responsible for reservoir fluid displacement and production, rather than making uninformed “engineering judgment” that is not based on known physics impacting fluid production from such reservoirs.

6.2 Recommendations and Future Work

More laboratory experiment should be carried out to properly characterize the behavior of the relative permeability curves and the end points values at low and high stress conditions for different class of reservoir materials. A further investigation of the response of the irreducible water saturation with decreasing/increasing effective stresses should also be carried out. Changes to the Corey's water and oil saturation exponent as a function of change in in-situ stress condition should also be investigated for different stress paths and included in a future work.

Lastly, while this work had been able to ultimately achieve the development of the procedure for coupling stress dependent relative permeability and reservoir simulation, further analysis should be conducted to obtain a more robust empirical equations for predicting stress-induced changes in relative permeability functions for low/high stresses, for both cemented/uncemented reservoir in different stress path.

References:

Al-Harthy S. S, Dennis J.W., Marsden J.R. 1998. Hysteresis, True triaxial Stress-Path and Pore Pressure Effects on Permeability. Eurock' 98 Conference, SPE/ISRM, vol. 47269. Norway, Trondheim.

Ali S., A. Al-Marhoun, A. Abu-Khamsin and S. Celik. 1987. The Effect of Overburden Pressure on Relative Permeability. SPE paper 1573.

Al-Quraishia A., M. Khairy. 2005. Pore Pressure versus Confining Pressure and their Effect on Oil–Water Relative Permeability Curves. Journal of Petroleum Science and Engineering, 48, pp. 120 – 126.

Archer, J.S., and Wong S.W. 1973. Use of a Reservoir Simulator To Interpret Laboratory Waterflood Data. SPE Journal, pp. 343-347, Dec.

Aziz K., and S. Antonin. 1979. Petroleum Reservoir Simulation. Applied Science Publishers Ltd, London. ISBN 0-85334-787-5.

Coates K. H. 1987. Reservoir Simulation. Hand Book of Petroleum Engineering, SPE., Richardson, T.X., pp. 48.1-48.5.

Coats K. H. 1968. Use and Misuse of Reservoir Simulation Models. Journal of Petroleum Technology, November, Volume: 21, Issue: 11, pp. 1391-1398.

CMG. 2008. IMEX 2008.12 User's Guide.

Dean, R., X. Gai, C. Stone, and S. Minkoff. 2003. A Comparison of Techniques for Coupling Porous Flow and Geomechanics. Paper SPE 79709, Presented at the SPE Reservoir Simulation Symposium, Houston, Texas, 3-5 February.

Geertsma, J. 1957. The effect of fluid Pressure Decline on Volumetric Changes of Porous Rocks. Trans AIME, 210, pp. 331-340.

Gutierrez M. and R.W. Lewis. 1998. The Role of Geomechanics in Reservoir Simulation. SPE/ISRM Eurock' 98, Trondheim, Norway, 8-10 July, pp. 439-448.

Gutierrez M., R.W. Lewis and I. Masters. 2001. Petroleum Reservoir Simulation Coupling Fluid Flow and Geomechanics. SPE Reservoir Evaluation & Engineering, June, pp. 164 - 172.

Gutierrez M and H. Hansteen. 1994. Fully Coupled Analysis of Reservoir Compaction and Subsidence. In: EUROPECS'94, London, UK, Paper SPE-28900.

Hamoud, M., R.J. Chalaturnyk and J. Leung. 2012. Influence of Geomechanical Processes on Relative Permeability. Canadian Rock Mechanics Symposium, Edmonton, Alberta, 9 p.

Heaviside J., C.J. Black and J. F. Berry. 1983. Fundamentals of Relative Permeability: Experimental and Theoretical Considerations. Paper 12173, 58th Annual meeting of SPE of AIME, San Francisco.

Hillestad J.G. 1986. Techniques for Simulating Complex Reservoir. International Meeting on Petroleum Engineering, 17-20 March, Beijing, China, SPE 14109.

Honarpour M., Koederitz L. and Harvery H. 1986. Relative Permeability of Petroleum Reservoirs. CRC Press, Inc Boca Raton, Florida. ISBN 0.8493-5739-X, pp. 1-15.

Honarpour M., S.M Mahmood. 1988. Relative-Permeability Measurements: An Overview. SPE, JPT, Today's Series, 963-966.

Hudson J.A., and J. Harrison. 1997. Engineering Rock Mechanics - An Introduction to Principles. First Edition 1997 Published by Elsevier Science Ltd, pp. 31-32, ISBN: 0 08 041912 7.

Itasca. 2010. FLAC3D 4.0 Manual.

Jin M., J. Somerville and B.D Smart. 2000. Coupled Reservoir Simulation Applied to the Management of Production Induced Stress-Sensitivity. SPE International Oil and Gas Conference and Exhibition, Beijing, 7-10 November, SPE 64790.

JOA. 2009. JewelSuite, User's Guide.

Jones, C., A. Al-Quraishi, J. Somerville1, S. Hamilton. 2001. Stress Sensitivity of Saturation and End-Point Relative Permeability. Paper presented at the International Symposium of the Society of Core Analysts, Edinburgh, Scotland, 17-19 September.

Longuemare, P., M. Mainguy, P. Lemonnier, A. Onaisi, C. Gerard, and N. Koutsabeloulis. 2002. Geomechanics in Reservoir Simulation - Overview of Coupling Methods and Field Case Study. Oil and Gas Science and Technology – Rev. IFP, Vol. 57, No. 5, pp. 471.

Khan, A. H. 2009. Shear Induced Relative Permeability Changes in Uncemented Sands. Masters of Science in Engineering Thesis, December 2009, University of Texas at Austin, USA.

Minkoff, S., M. Stone, S. Bryant, M. Peszynska, and M. Wheeler. 2003. Coupled Fluid Flow and Geomechanics Deformation Modeling. Journal of Petroleum Science and Engineering 38, pp. 37-56.

Morgan J.T., Gordon D.T. 1970. Influence of Pore Geometry on Water-Oil Relative Permeability. JPT, October, p. 1199-1208.

Nelson Inoue and Sergio A. B. da Fontoura. 2009. Answers to Some Questions about the Coupling between Fluid Flow and Rock Deformation in Oil Reservoirs. SPE/EAGE Reservoir Characterization and Simulation Conference, 19–21 October, Abu Dhabi, UAE, SPE 125760.

Li, P. and R.J Chalaturnyk. 2006. Coupled Reservoir Geomechanical Simulations for the SAGD Process. Journal of Canadian Technology, January, Volume 45, No. 1, pp. 33-40.

Li, P., R.J Chalaturnyk and M. Poliker. 2004. Issues with Reservoir Geomechanical Simulations of the SAGD Process. Journal of Canadian Petroleum Technology, May, Volume 43, No. 5, pp. 30-40.

Rodríguez, R. 2010. Inclusion of Geomechanics in Streamline Simulation. M.Sc Thesis, University of Alberta, Canada, pp. 22-33.

Rodrigues, L. G. 2009. Flow Simulation in a Deepwater Reservoir: Fault Leakage Analysis. PhD Dissertation, University of Alberta, Canada, pp. 8-43.

Rodrigues, L., B. Cunha and R.J Chalaturnyk. 2007. Modelling Geomechanics into Petroleum Reservoir Numerical Simulation. A Coupled Technique in a Water Injection Project. Petroleum Society's 8th Canadian International Petroleum Conference, Calgary, Alberta, Canada, Paper 2007-060

Oldakowski, K. 1994. Stress Induced Permeability Changes of Athabasca Oil sands. M.Sc Thesis, University of Alberta, Canada, pp. 139-157

Osorio G., H. Chen, L.W Teufel. 1999. Numerical Simulation of the Impact of Flow-Induced Geomechanical Response on the Productivity of Stress-Sensitive Reservoirs. SPE Reservoir Simulation Symposium, SPE 51929, Houston, Texas, USA, pp. 1-4

Osorio, G., H. Chen, L. Teufel and S. Schaffers. 1998. A Two-Domain, 3D, Fully Coupled Fluid-Flow/Geomechanical Simulation Model for Reservoirs with Stress-Sensitive Mechanical and Fluid-Flow Properties. Proceedings presented at Eurock 98, Trondheim. Norway. July 8-10, SPE/lSRM 47397, pp. 455-464.

Samier P., A. Onaisi, and G. Fontaine. 2003. Comparisons of Uncoupled and Various Coupling Techniques for Practical Field Examples. SPE Journal, Volume 11, 1 November, pp. 89-102, SPE-79698-PA.

Settari, A., and F.M. Mourits. 1998. A coupled Reservoir and Geomechanical Simulation System. SPE Journal, September 1998, pp. 219-226.

Settari, A. and D.A. Walters. 2001. Advances in Coupled Geomechanical and Reservoir Modeling with Applications to Reservoir Compaction. SPE Journal, Vol. 6, No. 3, September, pp. 334-342

Settari, A. and D.A. Walters. 1999. Advances in Coupled Geomechanical and Reservoir Modeling with Applications to Reservoir Compaction. Paper SPE 51927, presented at the 1999 SPE Reservoir Simulation Symposium, Houston, TX., February 14-17, 1999.

Settari, A. 2002. Reservoir Compaction. SPE Distinguish Author Series, J. Pet. Technol., August 2002, pp. 62-69.

Staggs H.M. and E.F. Herbeck. 1971. Reservoir Simulation Models – An Engineering Overview, JPT, Vol. 23, pp. 1428-1436.

Stone T., G. Bowen, P. Papanastasiou and J. Fuller. 2000. Fully Coupled Geomechanics in a Commercial Reservoir Simulator. SPE European Petroleum Conference, Paris, 24-25 October, pp. 45-52, SPE 65107.

Tarek Ahmed. 1990. Reservoir Engineering Hand Book. Second Edition, Gulf Professional Publishing, pp. 280-294, pp. 717-720.

Thomas L.K., L.Y Chin, R.G. Pierson and J.E. Sylte. 2003. Coupled Geomechanics and Reservoir Simulation. SPE Journal, Vol. 8, December, pp. 350-358.

Tortike, W.S. and Farouq Ali. 1993. Reservoir Simulation Integrated with Geomechanics. The Journal of Canadian Petroleum Technology. Volume 32, No.5, pp. 28-37.

Tran, D., L. Nghiem, and L. Buchanan. 2009. Aspect of Coupling between Petroleum Reservoir Flow and Geomechanics. 43rd U.S. Rock Mechanics Symposium and 4th U.S.-Canada Rock Mechanics Symposium, ARMA, pp. 09 – 89.

Tran, D., L. Nghiem and L., Buchanan. 2005. An overview of Iterative Coupling Between Geomechanical Deformation and Reservoir Flow. SPE/PS-CIM/CHOA 97879.

Wilson, J.W. 1956. Determination of Relative Permeability under Simulated Reservoir Conditions," A.I.Ch.E. Journal, March 1956. Vol. 2, No. 1, pp. 94-100.

Zoback, M. 2007. Reservoir Geomechanics. Cambridge University Press, ISBN-13: 9780521770699, pp. 378-384.

Appendix A – IMEX File

```
**********************************************************************************************************************
** Coupling of Stress Induced Change in Relative Permeability into Numerical Simulation
** ******************************************************************************************************************
RESULTS SIMULATOR IMEX 2008.12
FILENAMES OUTPUT INDEX-OUT MAIN-RESULTS-OUT
   *TITLE1  'WATER FLOODING'
*TITLE2  '2 WELLS WATERFLOOD OPERATION'
*TITLE3  'Uncoupled Case'
  *CASEID  'Uncoupled'
   **---INPUT/OUTPUT CONTROL SECTION-----------------------------------------------
     *INUNIT  *SI
**----RESERVOIR DESCRIPTION KEYWORD GROUP-----------------------------------------
OUTDIARY BRIEF
OUTDIARY PRESAQ
OUTDIARY HEADER 20
      *WRST          *TIME
      *WPRN    *WELL *TIME
      *WPRN    *GRID *TIME
      *OUTPRN  *WELL *LAYER
      *OUTPRN  *GRID *IMEXMAP *SG     *SO     *SW  *PRES
      *WSRF    *WELL *TIME
      *WSRF    *GRID *TIME
      *OUTSRF  *GRID *SG     *SO     *SW  *PRES
*INCLUDE 'CMGBuilder01_grid01.inc'
**$ Property: Permeability I (md)   Max: 100  Min: 5
PERMI KVAR
 5 100 3*20 100 2*20 100 2*20
**$ Property: Permeability J (md)   Max: 100  Min: 5
PERMJ KVAR
 5 100 3*20 100 2*20 100 2*20
**$ Property: Permeability K (md)   Max: 1  Min: 0.05
PERMK KVAR
 0.05 1 3*0.2 1 2*0.2 1 2*0.2
**$ Property: Net to Gross Ratio  Max: 1  Min: 1
NETGROSS CON            1
**$ Property: Porosity  Max: 0.27  Min: 0.27
POR CON         0.27
 *PRPOR  11825
  *CPOR   4.47E-7
   **---COMPONENT PROPERTIES-------------------------------------------------------
*MODEL *BLACKOIL
*TRES 60
*PVT *BG 1
**$        p        Rs       Bo         Bg      viso       visg           co
      101.325   0.55734   1.03598     1.14806   6.64964  0.0121416  4.35113e-006
      327.904   1.14518   1.03713     0.35336   6.45348  0.0121628  4.35113e-006
      554.482   1.79171    1.0384    0.208139   6.25072  0.0121892  4.35113e-006
       781.06   2.48133   1.03975    0.147175   6.04812   0.012219  4.35113e-006
      1007.64   3.20552   1.04118     0.11363   5.84912  0.0122518  4.35113e-006
      1234.22   3.95884   1.04267   0.0924025   5.65567   0.012287  4.35113e-006
       1460.8   4.73746   1.04422   0.0777615   5.46886  0.0123244  4.35113e-006
      1687.37   5.53856   1.04582   0.0670536   5.28927   0.012364  4.35113e-006
      1913.95    6.3599   1.04747   0.0588821   5.11716  0.0124055  4.35113e-006
      2140.53   7.19972   1.04916   0.0524417   4.95256   0.012449  4.35113e-006
      2367.11   8.05656   1.05089   0.0472352   4.79538  0.0124942  4.35113e-006
      2593.69    8.9292   1.05266   0.0429393   4.64543  0.0125413  4.35113e-006
      2820.27    9.8166   1.05446   0.0393347   4.50247   0.01259  4.35113e-006
      3046.84   10.7179   1.05631   0.0362671   4.36621  0.0126405  4.35113e-006
      3273.42   11.6322   1.05818   0.0336251   4.23636  0.0126927  4.35113e-006
         3500    12.559   1.06009   0.0313261   4.11261  0.0127465  4.35113e-006
         9800   41.8186    1.1236   0.0101741   2.17467  0.0149024  3.44698e-006
        16100   75.4241   1.20269  0.00596024   1.44796  0.0182039  1.80822e-006
        22400   111.871   1.29405  0.00441026   1.08373  0.0219979  1.17823e-006
        28700   150.488    1.3959  0.00368092  0.867833  0.0256549  8.54599e-007
        35000   190.883   1.50706  0.00327233  0.725712  0.0289508  6.60921e-007
*BWI 1.01631
*CVW 0
*CW 4.56897e-007
*DENSITY OIL 886.26
*DENSITY WATER 990.394
*REFPW 101.325
*VWI 0.516363
*GRAVITY GAS 0.65
**$ Property: PVT Type  Max: 1  Min: 1
PTYPE CON            1
   **---ROCK-FLUID DATA KEYWORD GROUP----------------------------------------------
      *ROCKFLUID
      *RPT 1
 *SWT
**$    Sw           krw             krow
   0.200000  0.000000 0.510200
   0.235714  0.000010 0.439917
   0.271429  0.000163 0.374841
   0.307143  0.000824 0.314970
   0.342857  0.002603 0.260306
   0.378571  0.006355 0.210848
   0.414286  0.013177 0.166596
   0.450000  0.024412 0.127550
```

```
   0.485714  0.041647 0.093710
   0.521429  0.066710 0.065077
   0.557143  0.101676 0.041649
   0.592857  0.148864 0.023428
   0.628571  0.210836 0.010412
   0.664286  0.290398 0.002603
   0.700000  0.390600 0.000000
 SLT
**$    Sl      krg     krog
   0.500000  0.477200 0.000000
   0.535714  0.411463 0.002603
   0.571429  0.350596 0.010412
   0.607143  0.294598 0.023428
   0.642857  0.243469 0.041649
   0.678571  0.197210 0.065077
   0.714286  0.155820 0.093710
   0.750000  0.119300 0.127550
   0.785714  0.087649 0.166596
   0.821429  0.060867 0.210848
   0.857143  0.038955 0.260306
   0.892857  0.021912 0.314970
   0.928571  0.009739 0.374841
   0.964286  0.002435 0.439917
   1.000000  0.000000 0.510200
   **---INITIALIZATION----------------------------------------------------------
*INITIAL
*USER_INPUT
*PRES *CON 11825
*PB *CON 3500
*SO *CON 0.8
*SW *CON 0.2
*DATUMDEPTH 1222.2
   **---NUMERICAL---------------------------------------------------------------
      *NUMERICAL
*DTMAX 30.
**MAXSTEPS  999                 ** Maximum number of time steps
** Normal maximum changes per time step
NORM PRESS 30
AIM THRESH 0.25 0.25
   **---WELL AND RUN DATA-------------------------------------------------------
DTMIN 1e-6
Run
TIME 0
**$
GROUP 'SAM'  ATTACHTO 'FIELD'
WELL 1  'PRO_01'  ATTACHTO 'SAM'
WELL 2  'INJ_01'  ATTACHTO 'SAM'
WELL  'PRO_01'
**$          rad  geofac  wfrac  skin
GEOMETRY  K    0.11 0.29    0.5  0
PERF GEO   'PRO_01'
**$ UBA    ff  Status  Connection
21 1 1 1. OPEN FLOW-TO 'SURFACE'
21 1 2 1. OPEN FLOW-TO 1
21 1 3 1. OPEN FLOW-TO 2
21 1 4 1. OPEN FLOW-TO 3
21 1 5 1. OPEN FLOW-TO 4
21 1 6 1. OPEN FLOW-TO 5
21 1 7 1. OPEN FLOW-TO 6
21 1 8 1. OPEN FLOW-TO 7
21 1 9 1. OPEN FLOW-TO 8
21 1 10 1. OPEN FLOW-TO 9
21 1 11 1. OPEN FLOW-TO 10
WELL  'INJ_01'
**$          rad  geofac  wfrac  skin
GEOMETRY  K    0.11 0.29    0.5  0
PERF GEO   'INJ_01'
**$ UBA    ff  Status  Connection
1 21 1 1. OPEN FLOW-TO 'SURFACE'
1 21 2 1. OPEN FLOW-TO 1
1 21 3 1. OPEN FLOW-TO 2
1 21 4 1. OPEN FLOW-TO 3
1 21 5 1. OPEN FLOW-TO 4
1 21 6 1. OPEN FLOW-TO 5
1 21 7 1. OPEN FLOW-TO 6
1 21 8 1. OPEN FLOW-TO 7
1 21 9 1. OPEN FLOW-TO 8
1 21 10 1. OPEN FLOW-TO 9
1 21 11 1. OPEN FLOW-TO 10
PRODUCER 'PRO_01'
OPERATE  MIN  BHP  4000.  CONT
OPERATE  MAX  STO 200.  CONT
MONITOR MIN STO 5 SHUTIN
MONITOR MAX GOR 500 SHUTIN
MONITOR MAX WCUT 0.95 SHUTIN
INJECTOR MOBWEIGHT 'INJ_01'
INCOMP  WATER
OPERATE  MAX  BHP 13019.  CONT
OPERATE  MAX  STW 800.  CONT REPEAT

SHUTIN 'INJ_01'
TIME 0.00001
WRST TNEXT
```

```
TIME 30
WRST TNEXT
TIME 60
TIME 547.5
WRST TNEXT
OPEN 'INJ_01'
INJECTOR MOBWEIGHT 'INJ_01'
INCOMP  WATER
OPERATE  MAX  BHP 13019.  CONT
OPERATE  MAX  STW 800.  CONT REPEAT
TIME 730
WRST TNEXT
TIME 9125
*STOP
```

Appendix B – FLAC3D Initialization File

```
; Generated by: comp1
; Generated: 3:33:25 PM 19/10/2011
; model to create reservoir geometry in FLAC3D_4.00 45
; Driver file to initialize the reservoir mechanical grid, pore pressure, temperature, gas contents, stresses and properties
 new
TITLE 'Coupled Reservoir Geom with IMEX and FLAC3D'
config fluid therm zextra 50
; see IO_porepress.fis, IO_temp.fis, IO_gascontent.fis
; functions in FLAC_RG_fist (fist = fish tank)
 SET fluid off
 SET thermal off
 SET mech on
 SET echo off
 ; load support functions
   call C:\Users\comp1\Desktop\DN_2\GM\GM3D\FLAC_RG_fist\IO_general.fis
   call C:\Users\comp1\Desktop\DN_2\GM\GM3D\FLAC_RG_fist\IO_mechprops.fis
   call C:\Users\comp1\Desktop\DN_2\GM\GM3D\FLAC_RG_fist\IO_porepress.fis
   call C:\Users\comp1\Desktop\DN_2\GM\GM3D\FLAC_RG_fist\IO_temp.fis
   call C:\Users\comp1\Desktop\DN_2\GM\GM3D\FLAC_RG_fist\IO_gascontent.fis
   call C:\Users\comp1\Desktop\DN_2\GM\GM3D\FLAC_RG_fist\IO_stress.fis
   call C:\Users\comp1\Desktop\DN_2\GM\GM3D\FLAC_RG_fist\IO_results.fis
 SET @_sim_tag = 'Coupled_1'
; build grid
 IMPGRID Coupled_1_mech_grid.dat usegivenids
 model fl_iso
prop biot_c 1. ; not used, but required
 model th_iso
 prop cond 1. sp 1. u_thc 1.  ; not used, but required
; set boundary and initial stress conditions
 call C:\Users\comp1\Desktop\DN_2\GM\GM3D\Coupled_1_b_fixed_cond.dat
 call C:\Users\comp1\Desktop\DN_2\GM\GM3D\Coupled_1_b_stress_cond.dat
 @_assign_mech_props_3d
 @_initial_stress
 @_ini_pp_t_gc ; not used yet, fish functions for faster gp pp, t, gc import
 SET echo on
  set grav 0. 0. -9.81
; initialize plots with a single step
   step 1
   call C:\Users\comp1\Desktop\DN_2\GM\GM3D\FLAC_RG_fist\plot.f3dat
 SET @_sim_name = '3d'
 SET @_tag = '0_o'
SET @_save_state = '_i'
 @_save_file
 @_solve
 @_ini_dis_vel
 SET @_tag = 0
 @_output_stress
 @_output_strain
SET @_save_state = '_f'
 @_save_file
```

Appendix C - Relative Permeability Module

```
'Sub create_rel_perm_tables()
Dim rel_perm_curve(14, 5) As Single
Dim Avg_Vol_Strain, mphi_2_mphi_0, Kro_o, Sor_o, Krw_o, Swi_o, Sgcon_o, Krg_o, Krog_o, Nw_o, No_o, Nog_o, Ng_o As Single
Dim Kro_c, Sor_c, Krw_c, swi_c, Sgcon_c, Krg_c, Krog_c, Nw_c, No_c, Nog_c, Ng_c, sw_i, sw_f, sw_inc, sl_i, sl_f, sl_inc As Single
Dim corey_coef_arr(100000, 13) As Single
' set up tables
' determine max zones
Application.ScreenUpdating = False
fr = Sheets("Rel_Perm_GB_ID").Cells(12, 5).End(xlDown).row
For r = 12 To fr
region = Sheets("Rel_Perm_GB_ID").Cells(r, 5).Value
If region > max_region Then
 max_region = region
End If
Next
rrr = max_region + 8  ' start row for rel perm table
' fill corey function array
For reg = 0 To max_region - 1
For arr = 2 To 12
 corey_coef_arr(reg, arr) = Sheets("REL_Perm_Model").Cells(reg + 4, arr + 1).Value
Next
 corey_coef_arr(reg, 0) = 0
 corey_coef_arr(reg, 1) = 1
Next
rr = rrr
'create txt
txt1 = "Region ID  "
txt2 = "Model Type  "
txt3 = "Avg Vol Strain  "
txt4 = "mphi_2_mphi_0  "
txt5 = "Kro  "
txt6 = "Sor  "
txt7 = "Krw  "
txt8 = "Swi  "
txt9 = "Nw  "
txt10 = "No  "
txt11 = "Nog  "
txt12 = "Ng  "
txt13 = "Sw"
txt14 = "Krw"
txt15 = "Krow"
txt16 = "Sl"
txt17 = "Krg"
txt18 = "Krog"
txt19 = "Original"
txt20 = "Previous"
txt21 = "Current"
txt22 = "Sgcon  "
txt23 = "Krg  "
txt24 = "Krog  "
txt25 = "2"
txt26 = "Step"
txt27 = "0"
  Sheets("REL_Perm_Model").Cells(rr + 4 + arr, 2).Value = corey_coef_arr(region - 1, arr)
Next
 If region = 1 Then
   format_rel_perm_tables (rrr)
 End If
 If region <> max_region Then
  Range(Cells(rr + 2, 1), Cells(rr + 16, 22)).Copy
  Cells(rr + 17, 1).Select
  ActiveSheet.Paste
 End If
rr = rr + 15
```

```
Next
' write rel perm curves functions
rr = rrr
For region = 1 To max_region
Avg_Vol_Strain = corey_coef_arr(region - 1, 0)
mphi_2_mphi_0 = corey_coef_arr(region - 1, 1)
Kro_o = corey_coef_arr(region - 1, 2)
Sor_o = corey_coef_arr(region - 1, 3)
Krw_o = corey_coef_arr(region - 1, 4)
Swi_o = corey_coef_arr(region - 1, 5)
Sgcon_o = corey_coef_arr(region - 1, 6)
Krg_o = corey_coef_arr(region - 1, 7)
Krog_o = corey_coef_arr(region - 1, 8)
Nw_o = corey_coef_arr(region - 1, 9)
No_o = corey_coef_arr(region - 1, 10)
Nog_o = corey_coef_arr(region - 1, 11)
Ng_o = corey_coef_arr(region - 1, 12)
'********** rel perm functions **********
Kro_c = Kro_o * (2.3578 * mphi_2_mphi_0 - 1.3962)
Sor_c = Sor_o * (5.2527 – 4.1089 * mphi_2_mphi_0)
Krw_c = Krw_o * (4.334 - 3.454 * mphi_2_mphi_0)
If mphi_2_mphi_0 < 1 Then
swi_c = Swi_o * (7.95 - 6.95 * mphi_2_mphi_0)
End If
If mphi_2_mphi_0 = 1 Then
swi_c = Swi_o * (7.95 - 6.95 * mphi_2_mphi_0)
End If
If mphi_2_mphi_0 > 1 Then
 swi_c = Swi_o * ((-35.15* mphi_2_mphi_0 - 2.8642^2)+ 76.72 * mphi_2_mphi_0-40.56)
End If
Sgcon_c = Sgcon_o
If swi_c < 0.15 Then
swi_c = 0.15
End If
If swi_c > 0.24 Then
swi_c = 0.24
End If
If Sor_c < 0.15 Then
Sor_c = 0.15
End If
If Sor_c > 0.36 Then
Sor_c = 0.36
End If
Krg_c = Krg_o
Krog_c = Krog_o
Nw_c = Nw_o
No_c = No_o
Nog_c = Nog_o
Ng_c = Ng_o
sw_i = swi_c
sw_f = 1 - Sor_c
If sw_f = 1 - Sor_c < 1 Then
   sw_f = 1 - Sor_c
   Else
sw_f = 1
 End If
sw_inc = (sw_f - sw_i) / 14
sl_i = Swi_o + Sor_c
sl_f = 1
sl_inc = (sl_f - sl_i) / 14
'********** write corey's functions **********
For sat = 0 To 14
'********** Water Oil Table **********
 rel_perm_curve(sat, 0) = sw_i + sat * sw_inc 'sw
 rel_perm_curve(sat, 1) = Krw_c * ((rel_perm_curve(sat, 0) - swi_c) / (1 - swi_c - Sor_c)) ^ Nw_c  ' Krw
 rel_perm_curve(sat, 2) = Kro_c * ((1 - rel_perm_curve(sat, 0) - Sor_c) / (1 - swi_c - Sor_c)) ^ No_c ' Kroc
 If sat = 0 Then
   rel_perm_curve(sat, 1) = 0
 End If
 If sat = 14 Then
```

```
  rel_perm_curve(sat, 2) = 0
End If
If rel_perm_curve(sat, 1) < 0 Then
  rel_perm_curve(sat, 1) = 0
ElseIf rel_perm_curve(sat, 1) > 1 Then
 rel_perm_curve(sat, 1) = 1
End If
If rel_perm_curve(sat, 2) < 0 Then
  rel_perm_curve(sat, 2) = 0
ElseIf rel_perm_curve(sat, 2) > 1 Then
 rel_perm_curve(sat, 2) = 1
End If

If sat = 13 Then
'  rel_perm_curve(sat, 3) = 1 - Sgcon_c
'  rel_perm_curve(sat, 4) = 0
End If
If sat = 14 Then
  'rel_perm_curve(14, 5) = rel_perm_curve(0, 2)
  'rel_perm_curve(14, 4) = 0
End If
If rel_perm_curve(sat, 4) < 0 Then
  rel_perm_curve(sat, 4) = 0
ElseIf rel_perm_curve(sat, 4) > 1 Then
 rel_perm_curve(sat, 4) = 1
End If
If rel_perm_curve(sat, 5) < 0 Then
  rel_perm_curve(sat, 5) = 0
ElseIf rel_perm_curve(sat, 5) > 1 Then
 rel_perm_curve(sat, 5) = 1
End If
Sheets("REL_Perm_Model").Cells(rr + 2 + sat, 6).Value = rel_perm_curve(sat, 3)
Sheets("REL_Perm_Model").Cells(rr + 2 + sat, 7).Value = rel_perm_curve(sat, 4)
Sheets("REL_Perm_Model").Cells(rr + 2 + sat, 8).Value = rel_perm_curve(sat, 5)
Next
rr = rr + 15
Next
 'fill the previous and current tables
fr = Cells(rrr + 2, 2).End(xlDown).row
Range(Cells(rrr + 2, 2), Cells(fr, 8)).Copy
Cells(rrr + 2, 9).Select
  ActiveSheet.Paste
Cells(rrr + 2, 16).Select
  ActiveSheet.Paste
Sheets("Simulation Control").Select
End Sub
```

Appendix D – Original (Khan, 2009) and Synthetic Data

Columns 2 to 7 contain Khan's (2009) original data while the entries in the rest of the column were synthesized.

Sand Type	*Strain*	*Ev*	*k*	Kro	Krw	Sor	Swi	ϕ	ϕ*	k*	Kro*	Krw*	Sor*	Swi*
Lower Fine Ottawa	0.000	0.000	6.2000	0.6000	0.0850	0.2300	0.1400	0.3200	1.0000	1.0000	1.0000	1.0000	1.0000	1.0000
Triaxial Test	1.000	-0.0025	5.5000	0.4500	0.0900	0.2700	0.1320	0.3183	0.9947	0.8878	0.7500	1.0588	1.1739	0.9429
	2.000	-0.0019	4.6000	0.4450	0.0820	0.2900	0.1280	0.3187	0.9959	0.7412	0.7417	0.9647	1.2609	0.9143
	3.000	0.0047	4.8500	0.4900	0.0780	0.3000	0.1530	0.3232	1.0099	0.7819	0.8167	0.9176	1.3043	1.0929
	5.000	0.0196	6.3000	0.6300	0.1000	0.2500	0.1780	0.3330	1.0408	1.0156	1.0500	1.1765	1.0870	1.2714
	10.000	0.0520	7.0000	0.6200	0.1500	0.1800	0.2080	0.3536	1.1050	1.1289	1.0333	1.7647	0.7826	1.4857
Lower Fine Ottawa	0.000	0.0000	5.6000	0.6000	0.1600	0.2270	0.1500	0.3260	1.0000	1.0000	1.0000	1.0000	1.0000	1.0000
Radial Extension Test	2.000	0.0451	6.8000	0.6100	0.1700	0.1800	0.1800	0.3551	1.0892	1.2143	1.0167	1.0625	0.7930	1.2000
	5.000	0.0774	7.7000	0.7600	0.2300	0.1560	0.1700	0.3744	1.1485	1.3750	1.2667	1.4375	0.6872	1.1333
	10.000	0.1000	8.4500	0.7500	0.2900	0.1600	0.1900	0.3873	1.1880	1.5089	1.2500	1.8125	0.7048	1.2667
Lower Fine Ottawa	0.000	0.0000	4.2000	0.7250	0.1800	0.2000	0.2000	0.3260	1.0000	1.0000	1.0000	1.0000	1.0000	1.0000
@ 345 kPa	2.000	-0.0119	3.5000	0.7000	0.1450	0.2200	0.2190	0.3179	0.9751	0.8333	0.9655	0.8056	1.1000	1.0950
	5.000	-0.0198	3.1000	0.6600	0.1350	0.2400	0.2410	0.3124	0.9582	0.7381	0.9103	0.7500	1.2000	1.2050
	10.000	-0.0241	2.9000	0.6300	0.1180	0.2800	0.2780	0.3093	0.9488	0.6905	0.8690	0.6556	1.4000	1.3900
Lower Ottawa	0.000	0.0000	4.5000	0.5500	0.1800	0.2000	0.2000	0.3270	1.0000	1.0000	1.0000	1.0000	1.0000	1.0000
@ 1379 kPa	2.000	0.0377	5.0000	0.6000	0.1450	0.2200	0.2200	0.3515	1.0748	1.1111	1.0909	0.8056	1.1000	1.1000
Radial Extension Test	5.000	0.0539	5.6000	0.6600	0.1340	0.2400	0.2400	0.3614	1.1053	1.2444	1.2000	0.7444	1.2000	1.2000
	10.000	0.0591	6.1000	0.6800	0.1180	0.2800	0.2800	0.3646	1.1148	1.3556	1.2364	0.6556	1.4000	1.4000
Lower Amalgamated	0.000	0.0000	20.0000	0.5300	0.1100	0.2400	0.1000	0.3170	1.0000	1.0000	1.0000	1.0000	1.0000	1.0000
Triaxial Test	1.000	-0.0047	18.0000	0.5100	0.0856	0.2700	0.0950	0.3138	0.9898	0.9000	0.9623	0.7782	1.1250	0.9500
	2.000	-0.0038	16.5000	0.4800	0.0900	0.2900	0.0800	0.3144	0.9919	0.8250	0.9057	0.8182	1.2083	0.8000
	3.000	0.0017	15.2000	0.4300	0.0800	0.3400	0.0400	0.3182	1.0036	0.7600	0.8113	0.7273	1.4167	0.4000
	5.000	0.0218	21.5000	0.5900	0.1300	0.2500	0.1300	0.3316	1.0460	1.0750	1.1132	1.1818	1.0417	1.3000
	10.000	0.0458	22.9000	0.6700	0.1350	0.1800	0.1600	0.3469	1.0944	1.1450	1.2642	1.2273	0.7500	1.6000
Lower Amalgamated	0.000	0.0000	19.0000	0.5300	0.1300	0.2400	0.1100	0.3280	1.0000	1.0000	1.0000	1.0000	1.0000	1.0000
Radial Extension Test	2.000	0.0403	22.3000	0.6200	0.1500	0.2000	0.1500	0.3540	1.0794	1.1737	1.1698	1.1538	0.8333	1.3636
	5.000	0.0663	23.8000	0.6900	0.1900	0.1200	0.1300	0.3698	1.1274	1.2526	1.3019	1.4615	0.5000	1.1818
	10.000	0.0932	25.7200	0.6800	0.2150	0.1150	0.1200	0.3853	1.1747	1.3537	1.2830	1.6538	0.4792	1.0909
Medium Ottawa	0.000	0.0000	35.0000	0.7000	0.2300	0.2300	0.0900	0.3257	1.0000	1.0000	1.0000	1.0000	1.0000	1.0000
Triaxial Test	1.000	-0.0060	32.4000	0.6600	0.1800	0.2600	0.0800	0.3217	0.9876	0.9257	0.9429	0.7826	1.1304	0.8889
	2.000	-0.0070	30.0000	0.6200	0.1500	0.2800	0.0700	0.3210	0.9855	0.8571	0.8857	0.6522	1.2174	0.7778
	3.000	-0.0005	27.5000	0.4900	0.1450	0.2950	0.0680	0.3254	0.9989	0.7857	0.7000	0.6304	1.2826	0.7556
	5.0000	0.0207	36.0000	0.7547	0.1700	0.2100	0.1000	0.3394	1.0420	1.0286	1.0781	0.7391	0.9130	1.1111
	10.000	0.0417	38.0000	0.7700	0.2500	0.1700	0.1100	0.3527	1.0829	1.0857	1.1000	1.0870	0.7391	1.2222
Medium Ottawa	0.000	0.0000	30.0000	0.5500	0.1700	0.2600	0.1000	0.3170	1.0000	1.0000	1.0000	1.0000	1.0000	1.0000
Radial Extension Test	2.000	0.0446	31.5000	0.6400	0.1900	0.2200	0.1300	0.3462	1.0920	1.0500	1.1636	1.1176	0.8462	1.3000
	5.000	0.0673	33.0000	0.6900	0.2800	0.1740	0.1500	0.3601	1.1359	1.1000	1.2545	1.6471	0.6692	1.5000
	10.000	0.0862	35.9200	0.7200	0.2900	0.1500	0.1400	0.3712	1.1710	1.1973	1.3091	1.7059	0.5769	1.4000

Table D-1: Triaxial compression and radial extension data

Appendix E – Fluid Properties

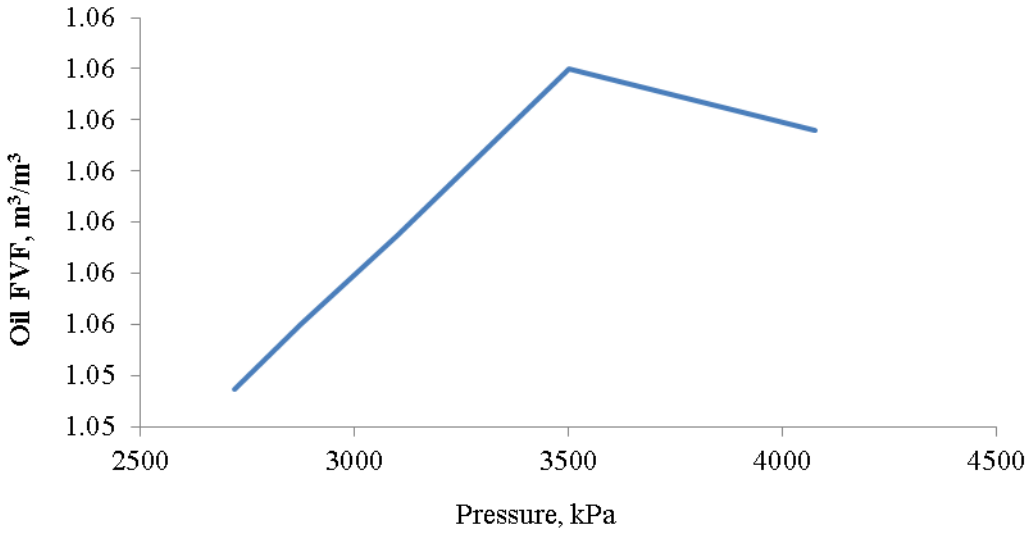

Figure E.1: Oil formation volume factor vs. pressure.

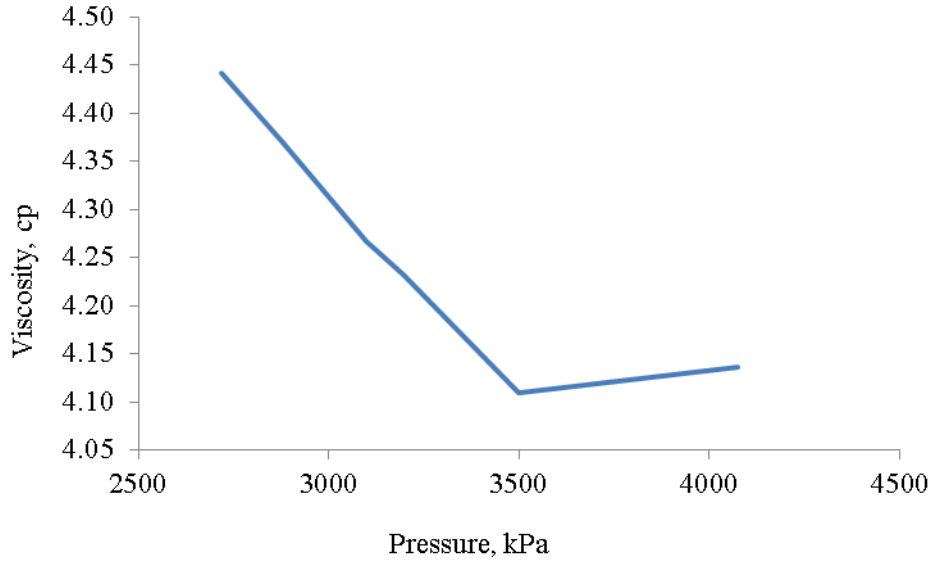

Figure E.2: Oil viscosity vs. pressure.

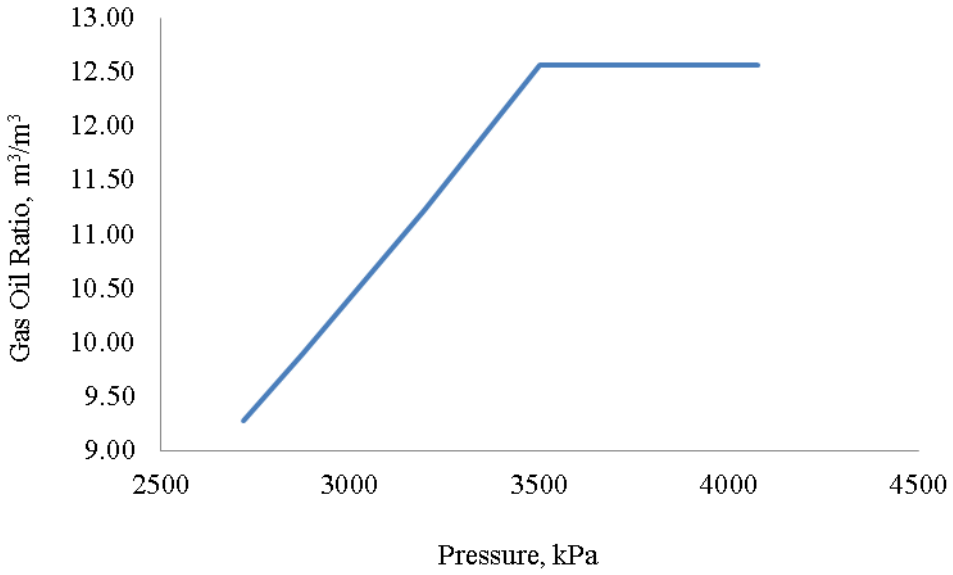

Figure E.3: Gas-oil ratio vs. pressure.